

1
 3
 2

4

Running as fast as it can: How spiking dynamics form object groupings in the laminar circuits of visual cortex

5

6

Jasmin Léveillé · Massimiliano Versace ·
 Stephen Grossberg

7

8

Received: 9 July 2009 / Revised: 15 December 2009 / Accepted: 30 December 2009

9

© Springer Science+Business Media, LLC 2010

10

Abstract How spiking neurons cooperate to control behavioral processes is a fundamental problem in computational neuroscience. Such cooperative dynamics are required during visual perception when spatially distributed image fragments are grouped into emergent boundary contours. Perceptual grouping is a challenge for spiking cells because its properties of collinear facilitation and analog sensitivity occur in response to binary spikes with irregular timing across many interacting cells. Some models have demonstrated spiking dynamics in recurrent laminar neocortical circuits, but not how perceptual grouping occurs. Other models have analyzed the fast speed of certain percepts in terms of a single feedforward sweep of activity, but cannot explain other percepts, such as illusory contours, wherein perceptual ambiguity can take hundreds of milliseconds to resolve by integrating multiple spikes over time. The current model reconciles fast feedforward with slower feedback processing, and binary spikes with analog network-level properties, in a laminar cortical network of spiking cells whose emergent properties quantitatively simulate parametric data from neurophysiological experiments, including the formation of illusory

contours; the structure of non-classical visual receptive fields; and self-synchronizing gamma oscillations. These laminar dynamics shed new light on how the brain resolves local informational ambiguities through the use of properly designed nonlinear feedback spiking networks which run as fast as they can, given the amount of uncertainty in the data that they process.

Keywords Perceptual grouping · Laminar cortical circuit · Spiking neuron · Visual cortex · Gamma oscillations · Illusory contour · Bipole cell

1 Introduction: Perceptual grouping in the laminar circuits of visual cortex

From spikes to behavior: The challenge posed by perceptual grouping Although many neurons communicate in the brain using discrete spikes, there are surprisingly few studies that show how spiking neurons cooperate to control behavioral processes. Such cooperative dynamics are required during visual perception when spatially distributed image fragments are grouped into emergent boundary contours. Grouping of local image contrasts is an important step in the perceptual organization process that leads to the emergence of 3D object boundary representations. Such boundaries delimit object borders and surfaces, allowing the brain to build meaningful perceptual units in response to complex scenes, and thereby contributing to global form perception. While perceptual grouping has long been studied in psychology, and several models of perceptual grouping have been proposed, it remains necessary to fully characterize the mechanisms and functions in laminar cortical circuits whose cell communicate via spiking dynamics. In particular, although models have been

Action Editor: B. A. Olshausen

J. Léveillé · M. Versace · S. Grossberg
 Department of Cognitive and Neural Systems,
 Center for Adaptive Systems, Boston University,
 677 Beacon Street,
 Boston, MA 02215, USA

J. Léveillé · M. Versace · S. Grossberg (✉)
 Center of Excellence for Learning in Education, Science,
 and Technology, Boston University,
 677 Beacon Street,
 Boston, MA 02215, USA
 e-mail: steve@bu.edu

64 introduced that begin to explain how spiking neurons
 65 within laminar circuits of visual cortex support certain
 66 perceptual and cognitive processes, spiking laminar models
 67 of perceptual grouping remain to be characterized.

68 Illusory contour stimuli illustrate the requirements that
 69 must be satisfied by an adequate grouping mechanism.
 70 Illusory contours show that perceptual boundaries are
 71 completed only in regions enclosed by properly aligned
 72 boundary inducers. As described in greater detail below,
 73 some models have demonstrated spiking dynamics in
 74 recurrent laminar neocortical circuits, but not how percep-
 75 tual grouping occurs. Other models have analyzed the fast
 76 speed of certain percepts in terms of a single feedforward
 77 sweep of activity, but cannot explain other percepts, such as
 78 illusory contours, wherein perceptual ambiguity can take
 79 hundreds of milliseconds to resolve by integrating multiple
 80 spikes over time. The current model reconciles fast
 81 feedforward with slower feedback processing, and binary
 82 spikes with analog network-level properties, in a laminar
 83 cortical network of spiking cells whose emergent properties
 84 quantitatively simulate parametric data from neurophysio-
 85 logical experiments, including the formation of illusory
 86 contours; the structure of non-classical visual receptive
 87 fields; and self-synchronizing gamma oscillations. These
 88 laminar dynamics shed new light on how the brain resolves
 89 local informational ambiguities through the use of properly
 90 designed nonlinear feedback networks that run as fast as
 91 they can, given the amount of uncertainty in the data that
 92 they process, and automatically slow down processing to
 93 use internal feedback processes to resolve informational
 94 ambiguities before speeding up again. In other words, the
 95 brain is designed in many situations to trade informational
 96 uncertainty against speed.

97 A classical example of an illusory contour is shown in
 98 Fig. 1(a). Here, a Kanizsa square stimulus with four
 99 pacmen inducers leads to the percept of a bright square
 100 bounded by illusory contours. A parsimonious explanation
 101 is that neural signals corresponding to almost collinear
 102 pairs of edge inducers complete over the gap that separates them,
 103 as reported in the neurophysiological data of von der Heydt
 104 et al. (1984) and Peterhans and von der Heydt (1989),
 105 among others (see Table 1). A key problem to solve is why
 106 illusory contours do not propagate from a single image
 107 inducer. Were this possible, then every dot in an image
 108 could propagate uncontrollably in all directions to fill the
 109 image percept. This does not occur because *inward*
 110 boundary completion between pairs or greater numbers of
 111 inducers, on opposite sides of a target cell, occurs without
 112 causing uncontrollable *outward* boundary propagation from
 113 a single inducer. This has been called the *bipole grouping*
 114 *property* in the Boundary Contour System, or BCS, model
 115 of perceptual grouping and boundary completion that was
 116 introduced by Grossberg and his colleagues (e.g., Cohen

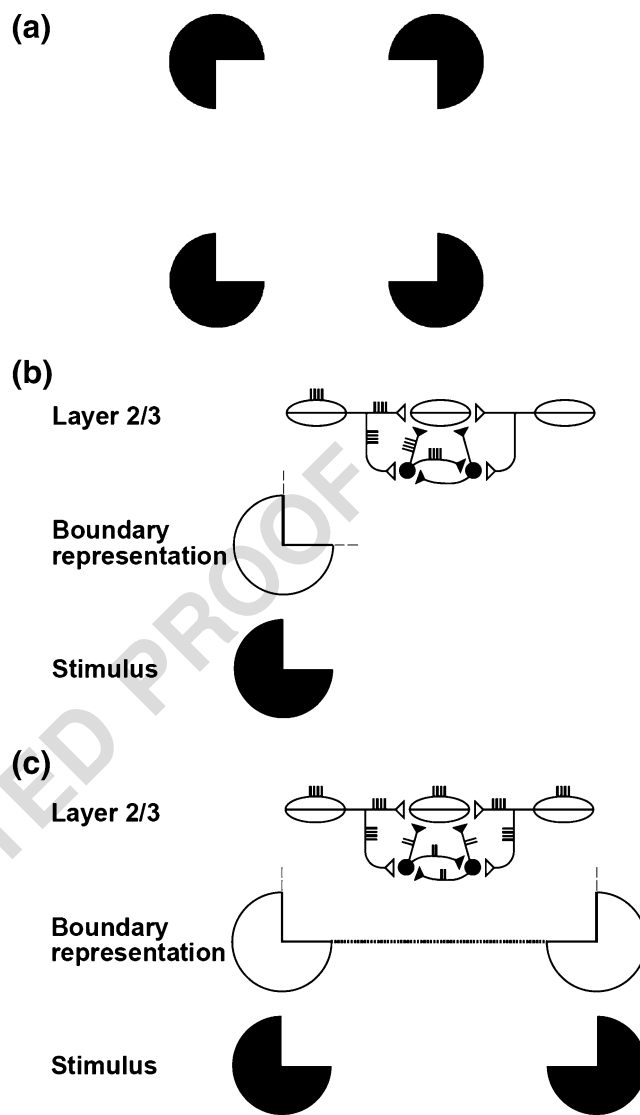


Fig. 1 Perceptual grouping by bipole cell interactions: (a) The four pac man figures induce the percept of a Kanizsa square whose sides are delimited by illusory contours. (b) Input from a single pac man is insufficient to induce illusory contours. (c) Input from a pair of collinear pac man edges creates an illusory contour by activating bipole cells at all positions between them

and Grossberg 1984; Grossberg 1984; Grossberg and
 Mingolla 1985a, b). Psychophysical experiments on asso-
 ciation fields (Field et al. 1993) and contour interpolation
 (Kellman and Shipley 1991), among others, have supported
 the bipole grouping concept.

The more recent 3D LAMINART model has refined the
 analysis of bipole grouping by predicting how it takes place
 in laminar cortical circuits, and has thereby explained much
 larger psychophysical and neurobiological data bases that
 depend upon perceptual grouping, including properties of
 cortical development, perceptual learning, attention, 3D
 vision, figure-ground separation, and perceptual bistability,
 including Necker cube bistability and binocular rivalry

Q1

t1.1 **Table 1** Model connections and supporting anatomical data

t1.2	Model connection	Functional interpretation	Selected references
t1.3	LGN → 4	Strong LGN input	Blasdel and Lund (1983); Ferster et al. (1996); Thomson and Bannister (2003)
t1.4	4 → 2/3 pyramidal	Feedforward stimuli with bottom-up support	Fitzpatrick (1996); Callaway and Wiser (1996); Shmuel et al. (2005)
t1.5	V1 2/3 pyr. → 2/3 pyr.	Long-range collinear integration	Bosking et al. (1997); Schmidt et al. (1997); Chisum et al. (2003)
t1.6	V2 2/3 pyr. → 2/3 pyr.	Long-range collinear integration	Levitt et al. (1994)
t1.7	2/3 pyr. → 2/3 inhib. int.	Keep outward grouping subthreshold (bipole property)	McGuire et al. (1991); Hirsch and Gilbert (1991); Holmgren et al. (2003)
t1.8	2/3 inhib. int. → 2/3 pyr.	Keep outward grouping subthreshold (bipole property)	Lund et al. (2001)
t1.9	2/3 inhib. int. → 2/3 inhib. int.	Normalize 2/3 inhibition (2-against-1 principle)	Tamas et al. (1998); Fukuda et al. (2006)

130 (e.g., Cao and Grossberg 2005; Fang and Grossberg 2009;
 131 Grossberg and Raizada 2000; Grossberg and Swaminathan
 132 2004; Grossberg and Williamson 2001; Grossberg and
 133 Yazdanbakhsh 2005; Grossberg et al. 2008; Yazdanbakhsh
 134 and Grossberg 2004). However, neurons in these laminar
 135 cortical models use rate coding, rather than spikes, to
 136 represent intercellular signals.

137 The present article models how perceptual grouping of
 138 boundaries emerges in a laminar cortical model of spiking
 139 neurons. Spiking neurons challenge the bipole property
 140 because communication using temporally discrete, not
 141 necessarily coincident, spikes from multiple cells increases
 142 the difficulty of computing whether two or more inducers
 143 are contributing to the formation of grouping. Indeed,
 144 multiple cells with different axonal delays contribute to
 145 boundary completion on either side of a target cell, yet a
 146 target bipole cell must somehow distinguish whether spikes
 147 converge on it from opposite sides of its cell body (which
 148 may cause boundary completion) or from a single side
 149 (which does not cause boundary completion). Just the fact
 150 of spike coincidence cannot explain this distinction.

151 *Reconciling fast feedforward and slower feedback proces-*
 152 *sing* Some recent models and experimental studies chal-
 153 lenge the idea that visual contours emerge through gradual
 154 accumulation of feedforward and feedback signals over
 155 time. Some models postulate that contours are represented
 156 by neurons that emit coincident spikes, rather than by the
 157 strength of their firing rates (Yen et al. 1999). Others
 158 hypothesize that the first feedforward wave of activity
 159 following stimulus onset is sufficient to represent boundary
 160 contours (VanRullen et al. 2001). Consistent with this
 161 perspective, face-selective neurons in primate inferotemporal
 162 cortex show significant selectivity for a target face 80–100 ms
 163 after stimulus onset (Oram and Perrett 1992). Such results are
 164 claimed to support a view of the brain in which perception is
 165 the result of a single feedforward wave of activity where

retinal input to LGN, V1, V2 and V4, and to IT takes no 166
 more than 10 ms between successive synaptic stages. Due to 167
 this stringent limit on processing time, it has been suggested 168
 that the order at which neurons in a population emit their 169
 first spike after stimulus onset, rather than their firing rate, 170
 codes for various dimensions of that stimulus (Thorpe et al. 171
 2001; VanRullen et al. 2005). 172

173 On the other hand, such a view is not compatible with a 173
 large number of perceptual experiments. For example, 174
 psychophysical experiments that have tried to estimate the 175
 amount of time required for illusory contour completion 176
 have yielded much slower processing times. One paradigm 177
 is that of primed-matching, in which a contour prime is 178
 presented prior to a test pair, and where the subject's task is 179
 to indicate whether the stimuli in the test pair are the same 180
 or not. Contour completion time is assessed by measuring 181
 how long an illusory contour prime must be presented for 182
 its priming effect to reach the same level as that of a 183
 corresponding real contour prime. In an initial study 184
 employing this paradigm, completion times of 75–200 ms 185
 were found (Sekuler and Palmer 1992). A later study 186
 highlighted the dependence of completion time on the size 187
 of the illusory contour gap, such that completion took 188
 somewhere between 255 and 450 ms for the largest gap 189
 studied in that experiment (Guttman et al. 2003). Another 190
 method compared the decay of persistence between real and 191
 illusory contours. Whereas for real contours persistence 192
 duration diminishes monotonically as a function of stimulus 193
 presentation, for illusory contours, persistence increases up 194
 to a certain presentation time, after which persistence 195
 duration diminishes in a manner similar to real contours. 196
 The time at which the decay of an illusory contour starts to 197
 follow the same course as that of the real contour may be 198
 interpreted as the time required for contour completion. 199
 Based on this interpretation, Meyer and Ming (1988) found 200
 completion times nearing 250 ms. Shape discrimination 201
 tasks have also been used in which stimuli were chosen so 202

Q2

Q3

203 as to require boundary completion for proper discrimination.
204 Such tasks have yielded estimates in the 46–170 ms range,
205 depending on stimulus conditions and task particularities
206 (Murray et al. 2001; Ringach and Shapley 1996). Taken
207 together, estimates from these studies suggest that boundary
208 formation is much slower than what would be predicted by
209 the single feedforward spike hypothesis.

210 Contour bridging cells in V2 take approximately 80 ms
211 to respond to illusory contour inducers (Peterhans and von
212 der Heydt 1989), which suggests that their responses
213 emerge from a relatively slow process of temporal
214 integration. Furthermore, these data show that initial spikes
215 are followed by longer lasting and irregular spike trains,
216 possibly indicating the gradual build-up of a robust neural
217 representation, and rendering unlikely the suggestion that
218 strict temporal order codes for contours. In support of this
219 view, awake macaque V1 recordings during presentation of
220 figure-ground stimuli show that, although cortical cells
221 respond to the mere presence of visual features around
222 57.5 ms, their activity is affected by the presence of
223 boundaries only much later, at around 95.0 ms (Lamme et
224 al. 1999). Transcranial magnetic pulses applied to early
225 visual areas block the perception of briefly presented
226 stimuli even when applied up to 120 ms after stimulus
227 onset, by which time the feedforward sweep is already
228 completed (Lamme and Roelfsema 2000). Feedback may
229 also influence contour formation, as suggested by human
230 brain activation studies during processing of illusory
231 contour figures, which have consistently shown the
232 presence of a wave of feedback activation from temporal
233 areas to V1 and V2 (Halgren et al. 2003; Murray et al.
234 2002; Yoshino et al. 2006). Against what one might expect
235 from the single feedforward sweep model, higher level
236 cortical areas are activated rather early during stimulus
237 processing, thereby allowing for feedback to influence early
238 activity. This is illustrated, for example, by microelectrode
239 recordings in anesthetized monkey in V1, V2 and V3,
240 which reveal that they are affected by inactivation of MT in
241 the first 10 ms after onset of response (Hupé et al. 2001). At
242 an even higher level, MEG recordings obtained in an object
243 recognition task show activity related to correct recognition
244 in orbitofrontal cortex (OFC) 50 ms before it is found in
245 fusiform areas which is usually considered to be at a lower
246 level on the feedforward pathway. Moreover, synchrony
247 between OFC and occipital areas appears 80 ms after onset,
248 whereas it appears at 130 ms between OFC and fusiform
249 areas (Bar et al. 2006). This may be taken to suggest that
250 stable feedforward and feedback interactions involving
251 OFC settle in lower visual areas prior to higher level ones.

252 *Varieties of brain feedback: Intralaminar, interlaminar,*
253 *intercortical* Several types of cortical feedback need to be
254 distinguished in order to achieve conceptual clarity: Intra-

255 laminar feedback due to recurrent interactions within a
256 single layer of cells, interlaminar feedback from cells in
257 more superficial layers to deeper layers of a single cortical
258 area, and intercortical feedback between cortical areas,
259 which is often called top-down processing.

260 Early neural models proposed how intercortical top-
261 down attentive feedback can enhance ongoing dynamics
262 when it matches feedforward activity, or reset them
263 otherwise, and trigger fast learning during the match phase
264 (Carpenter and Grossberg 1993; Grossberg 1976a, b). This
265 Adaptive Resonance Theory, or ART, model also mathe-
266 matically proved how the initial feedforward choice of a
267 learned recognition category may be confirmed and
268 sharpened by top-down attentive feedback, but that unfa-
269 miliar information could drive a memory search for a new
270 category through an iterated reset process. In addition, more
271 resets may occur during a difficult “high vigilance”
272 discrimination task than an easier one. Familiar percepts
273 with little uncertainty could thus be recognized quickly,
274 whereas unfamiliar or more challenging percepts may
275 require longer processing times. Involvement of feedback
276 is therefore proportionally related to task difficulty. This
277 sort of effect was reported in recent electrophysiological
278 recordings in macaque V4 during a task wherein an animal
279 had to detect large (easy to detect) or small (hard to detect)
280 orientation changes of a Gabor stimulus, and under
281 different attentional conditions (stimulus attended vs.
282 unattended). Firing rates obtained were higher in the
283 attended condition than in the unattended condition for
284 hard trials, whereas this difference was smaller for easy
285 trials. (Boudreau et al. 2006). A related proposal, based
286 primarily on perceptual learning studies and summarized as
287 the Reverse Hierarchy Theory (RHT), is that late feedback
288 to low level areas is necessary to refine a crude initial guess
289 at feature binding (Hochstein and Ahissar 2002).

290 Laminar cortical models enable a finer analysis of
291 intracortical processing. The circuitry of the LAMINART
292 model (Fig. 2; Grossberg 1999, 2003, 2007; Grossberg and
293 Todorović 1988; Grossberg and Raizada 2000; Raizada and
294 Grossberg 2001, 2003; Yazdanbakhsh and Grossberg 2004)
295 shows how a fast feedforward sweep of activation
296 throughout a cortical hierarchy could occur in response to
297 unambiguous information, consistent with the results of
298 Thorpe et al. (2001); see Fig. 2(e) wherein layers 4-to-2/3
299 in one cortical area project to layers 4-to-2/3 in the next,
300 and so on. However, in response to ambiguous information,
301 self-normalizing competition among alternative cortical
302 interpretations of the data may weaken the activation
303 amplitude and coherence of each alternative, thereby
304 slowing down its processing, and enabling interlaminar,
305 but intracortical, feedback (Fig. 2(c)) to contrast-enhance
306 and thereby choose the alternatives that are supported by
307 the most evidence, thereupon automatically speeding up

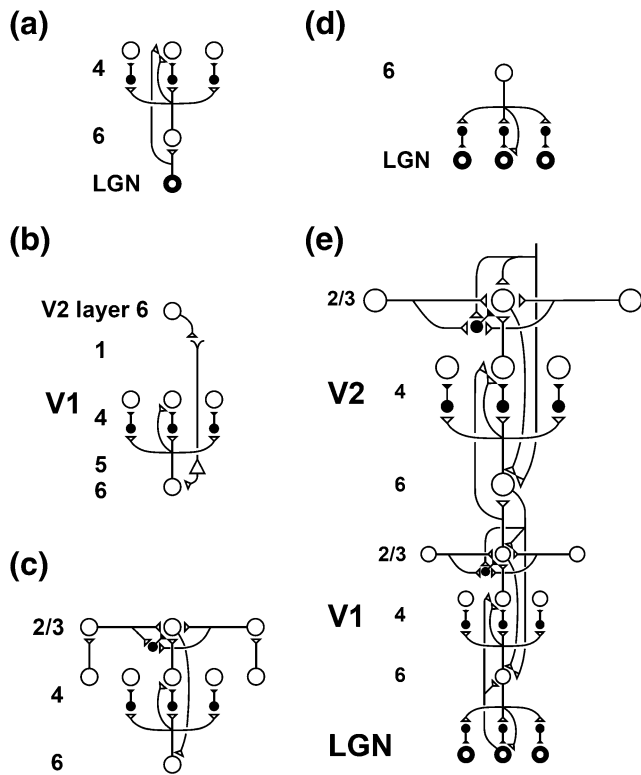


Fig. 2 How known cortical connections join layer 6 → 4 and layer 2/3 building blocks to form an entire V1/V2 LAMINART model. Inhibitory interneurons are shown *filled-in black*. (a) The LGN provides bottom-up activation to layer 4 via two routes. Firstly, it makes a strong connection directly into layer 4. Secondly, LGN axons send collaterals into layer 6, and thereby also activate layer 4 via the 6 → 4 on-center off-surround path. Thus, the combined effect of the bottom-up LGN pathways is to stimulate layer 4 via an on-center off-surround, which provides divisive contrast normalization (Grossberg 1973, 1980; Heeger 1992) of layer 4 cell responses. (b) Folded feedback carries attentional signals from higher cortex into layer 4 of V1, via the modulatory 6 → 4 path. Corticocortical feedback axons tend preferentially to originate in layer 6 of the higher area and to terminate in the lower cortex's layer 1 (Salin and Bullier 1995, p.110), where they can excite the apical dendrites of layer 5 pyramidal cells whose axons send collaterals into layer 6 (the *triangle* in the figure represents such a layer 5 pyramidal cell). Several other routes through which feedback can pass into V1 layer 6 exist. Having arrived in layer 6, the feedback is then “folded” back up into the feedforward stream by passing through the 6 → 4 on-center off-surround path (Bullier et al. 1996). (c) Connecting the 6 → 4 on-center off-surround to the layer 2/3 grouping circuit: like-oriented layer 4 simple cells with opposite contrast polarities compete (not shown) before generating half-wave rectified outputs that converge onto layer 2/3 complex cells in the column above them. Like attentional signals from higher cortex, groupings which form within layer 2/3 also send activation into the folded feedback path, to enhance their own positions in layer 4 beneath them via the 6 → 4 on-center, and to suppress input to other groupings via the 6 → 4 off-surround. There exist direct layer 2/3 → 6 connections in macaque V1, as well as indirect routes via layer 5. (d) Top-down corticogeniculate feedback from V1 layer 6 to LGN also has an on-center off-surround anatomy, similar to the 6 → 4 path. The on-center feedback selectively enhances LGN cells that are consistent with the activation that they cause (Silito et al. 1994), and the off-surround contributes to length-sensitive (endstopped) responses that facilitate grouping perpendicular to line ends. (e) The entire V1/V2 circuit: V2 repeats the laminar pattern of V1 circuitry, but at a larger spatial scale. In particular, the horizontal layer 2/3 connections have a longer range in V2, allowing above-threshold perceptual groupings between more widely spaced inducing stimuli to form (Amir et al. 1993). V1 layer 2/3 projects up to V2 layers 6 and 4, just as LGN projects to layers 6 and 4 of V1. Higher cortical areas send feedback into V2 which ultimately reaches layer 6, just as V2 feedback acts on layer 6 of V1 (Sandell and Schiller 1982). Feedback paths from higher cortical areas straight into V1 (not shown) can complement and enhance feedback from V2 into V1. [Reprinted with permission from Raizada and Grossberg 2001.]

308 processing of those choices. These properties clarify an
 309 important sense in which the cortex “runs as fast as it can”
 310 given the degree of uncertainty in the data. It also shows
 311 how the brain goes beyond current Bayesian models to
 312 implement a kind of real-time probability theory and
 313 hypothesis testing that can deal with ambiguous environ-
 314 ments whose rules can change rapidly through time.

315 In particular, the LAMINART model clarifies how a real
 316 boundary in an image may be formed with a fast
 317 feedforward sweep of activation from layers 4-to-2/3 and
 318 then on to layers 4-to-2/3 in subsequent cortical areas. In
 319 contrast, completion of an *unambiguous* illusory contour
 320 would require intralaminar feedback within a recurrent
 321 network using long-range horizontal connections within
 322 layer 2/3 (Fig. 2(c)), and could thus take considerably
 323 longer. Completion of an *ambiguous* illusory contour in an
 324 image with multiple possible groupings could, in addition
 325 to intralaminar feedback within layer 2/3, use interlaminar
 326 feedback between layers 2/3, 6, and 4 (Fig. 2(c)) to resolve
 327 the ambiguity. Feedback from the deeper 6-to-4 layers
 328 includes self-normalizing competitive interactions that,
 329 along with the positive feedback within layer 2/3 and
 330 between layers 2/3-to-6-to-4, help to choose among
 331 possible perceptual groupings. In addition, during both real
 332 and illusory contour formation, such a laminar cortical
 333 circuit may use intralaminar long-range interactions and
 334 interlaminar competitive interactions to synchronize signals
 335 that may be temporally dispersed due to different axonal
 336 and synaptic delays (Yazdanbakhsh and Grossberg 2004).

337 However, all of these results about boundary completion
 338 and illusory contour formation used rate-based models.
 339 What cortical mechanisms allow the bipole property to be
 340 realized in a spiking milieu? It is not sufficient to base such
 341 an analysis on the possibility that individual spikes may be
 342 coincident if only because outputs from multiple cells at
 343 multiple distances and time lags input to each bipole
 344 grouping cell from each side of its receptive field, and
 345 because the time scale of conscious perceptual grouping is
 346 orders of magnitude slower than the time scale of individual
 347 spiking coincidences.

348 Our study extends the LAMINART model to explain
 349 and quantitatively simulate parametric neurophysiological
 350 data about how spike-based cortical grouping may occur.
 351 This extended model represents a synthesis of the LAMI-

Q6

352 NART model and the Synchronous Matching ART
 353 (SMART) model of Grossberg and Versace (2008). The
 354 SMART model has already simulated how spiking dynamics
 355 in laminar cortical circuits can explain databases other than
 356 those about perceptual grouping. In particular, SMART
 357 clarifies how bottom-up adaptive filtering and top-down
 358 attentive learned expectation processes undergo match/
 359 mismatch operations that attentively regulate perceptual and
 360 cognitive processes, notably how multiple stages of laminar
 361 cortical processing interact with specific and nonspecific
 362 thalamic nuclei to control category learning and recognition,
 363 and how gamma and beta oscillations may be triggered in
 364 match and mismatch states, respectively. The current study
 365 focuses on the horizontal interactions that support perceptual
 366 grouping, rather than the bottom-up/top-down processes that
 367 regulate attention. A future study will synthesize both types of
 368 processes into a more comprehensive cortical model of how
 369 spiking dynamics are regulated in bottom-up, horizontal, and
 370 top-down laminar interactions.

371 Previous LAMINART modeling work simulated how
 372 cortical layer 2/3 pyramidal cells respond to inputs from
 373 deeper cortical layers to group together (almost) collinear
 374 image features via long-range recurrent excitatory interactions
 375 between the pyramidal cells. This long-range oriented
 376 interaction limits contextual contributions to a restricted set
 377 of neighboring collinear layer 2/3 cells with a similar
 378 orientation preference and (almost) collinear positional
 379 alignment, as has been experimentally found (Table 1).
 380 Figure 1(c) illustrates how a pair of collinear pac man
 381 figures can activate bipole cells located between them to
 382 form an illusory contour. Similar grouping kernels have been
 383 reported by several authors (e.g. Field et al. 1993; Li 1998).
 384 If only excitatory recurrent connections existed, run-away
 385 excitation could easily occur. This is prevented by balancing
 386 recurrent interactions between layer 2/3 long-range excitatory
 387 pyramidal cells and short-range inhibitory interneurons.
 388 Together, these inhibitory and excitatory interactions ensure
 389 that single-sided input, however strong, does not lead to
 390 horizontal activation (Fig. 1(b)). An excitatory-inhibitory
 391 balance also implies that inhibition is not too strong, thereby
 392 preventing maladaptive suppression of network activation.
 393 Earlier modeling has shown how such an excitatory-
 394 inhibitory balance can self-organize during cortical develop-
 395 ment and give rise to a laminar perceptual grouping circuit
 396 whose properties match perceptual data from adult human
 397 observers (Grossberg and Williamson 2001). This analysis
 398 illustrates how adult perceptual properties may emerge from
 399 the dynamics that govern stable brain development.

400 The distinction between the initial feedforward sweep
 401 and subsequent feedback interactions in the processing of
 402 contours is illustrated in Fig. 3, where interneurons have
 403 been omitted for clarity. Bottom-up input to layer 2/3 bipole
 404 cells is provided by cells in layer 4 (see also Fig. 4). In the

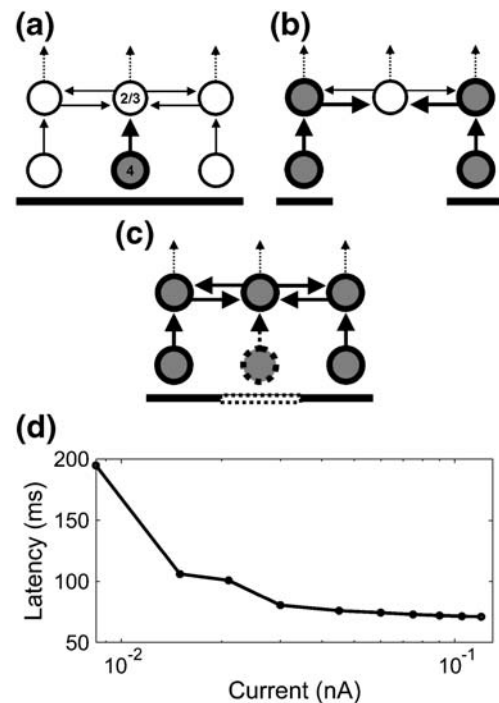


Fig. 3 Feedforward and feedback interactions in the bipole network for real and illusory contours. (a) Upon presentation of a real contour, a single feedforward wave of activity is sufficient to activate a bipole cell located in the middle of the contour via direct input from layer 4 (indicated in gray). (b) In comparison, bipoles located over an illusory contour gap receive only indirect excitation through layer 2/3 horizontal connections during the initial feedforward wave. This results in an increase in latency until the first middle bipole spike, compared to the real contour case. (c) After initial feedforward propagation, horizontal feedback from the middle bipoles in layer 2/3 contributes to strengthen boundary representations whether for real or illusory contours (denoted as dashed lines). (d) Difference between illusory and real contours in the latency of the first spike of the bipole cell located in the middle of the contour. The first spike always occurs later for illusory contours and at all current inputs, due to indirect activation through horizontal connections in the first feedforward wave of activation

case of a real contour (Fig. 3(a)), the first feedforward sweep activates layer 2/3 bipoles at all input-recipient cells, since each bipole cell then receives direct bottom-up input from layer 4. In the case of an illusory contour (Fig. 3(b)), the bipoles that are located over the illusory contour gap receive indirect input from neighboring bipoles after the latter are activated by the first feedforward sweep. A stable boundary representation then emerges due to subsequent recurrent feedback via horizontal connections within layer 2/3 (Fig. 3(c)). Because an illusory contour receives indirect horizontal input, rather than the more direct input to a real contour, the first spike occurs much later in the middle of an illusory contour than of a real contour (Fig. 3(d)). The results in Fig. 3(d) were obtained by simulating illusory and real contours and computing the difference in first spike latency of a cell located in the middle of the contour.

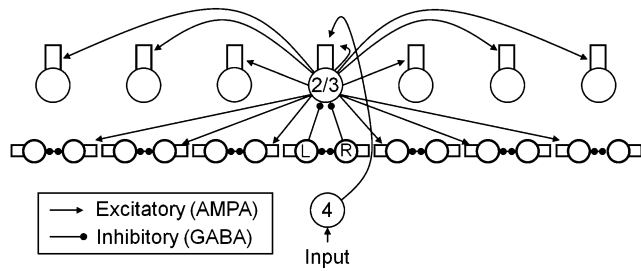


Fig. 4 Bipole cell circuit: Input is clamped at each spatial location at the level of Layer 4 pyramidal cells. Each layer 4 pyramidal cell projects to the dendrite of a single layer 2/3 pyramidal cell. The pyramidal cell dendrite also receives horizontal excitatory connections from neighboring layer 2/3 pyramidal cells, including projections from itself. Layer 2/3 horizontal connections also excite the dendrites of left or right inhibitory interneurons, which inhibit neighboring layer 2/3 pyramidal cell bodies and right or left inhibitory interneuron cell bodies. See Appendix Eqs. (11)–(17)

421 Nonzero input was applied at nine contiguous locations for
 422 the real contours, whereas the three locations in the middle
 423 were reset to zero for illusory contours. Both types of
 424 contours were simulated at current input strengths ranging
 425 between 0.0084 nA and 0.12 nA. The simulations indicate
 426 that the latency difference between illusory and real
 427 contours remains large (>50 ms) at all input strengths.

428 Feedback from higher cortical areas to lower ones
 429 enables interaction of grouping circuits at different spatial
 430 scales. For example, activation of smaller-scale bipole cells
 431 in V1 is modulated by feedback from larger-scale bipole
 432 cells in V2, such that contextual elements at a larger spatial
 433 scale may sharpen the activity at the level of V1 bipole cells
 434 (Anzai et al. 2007; Grossberg and Raizada 2000; Grossberg
 435 and Swaminathan 2004; Kisvárdy et al. 1997; Raizada and
 436 Grossberg 2001; Shmuel et al. 2005). Although this article
 437 models neurophysiological data about V1 horizontal inter-
 438 actions, the similarity of V1 and V2 circuits with respect to
 439 the presence of anisotropic horizontal collaterals suggests
 440 that variants of our results may also apply to V2. Table 2 lists
 441 supporting evidence from various species for the presence of
 442 bipole-type kernels in both V1 and V2. The kernels were
 443 chosen with the following considerations in mind: the extent
 444 of horizontal connections in layer 2/3, the approximate width
 445 of a hypercolumn, and the fact that each spatial location in
 446 the model represents one hypercolumn. Based on the data
 447 reviewed in Table 2, the extent of horizontal connections is
 448 estimated to be of approximately 7 mm, with a hypercolumn
 449 width of 1 mm, which is consistent with previous estimates
 450 (e.g. Yazdanbakhsh and Grossberg 2004). Based on these
 451 numbers, the horizontal kernels were chosen to span 7 spatial
 452 locations. Kernels of this size were also used in Grossberg
 453 and Swaminathan (2004).

454 The current Spiking LAMINART model (sLAMINART)
 455 uses Hodgkin-Huxley (1952) dynamics to represent realistic
 456 neuronal biophysical membrane constraints (cf. Gautrais

and Thorpe 1998). The model depends upon intracellular
 dynamics to temporally average across irregularities in
 individual spike timing, and to thereby enable bipole
 grouping to occur in response to approximately coincident
 bursts of spikes. The prevention of outward spreading of
 activation in response to individual image inducers also
 exploits spiking mechanisms. Hodgkin-Huxley type cells can
 behave as threshold units due to the presence of a stable
 attractor state during a period with little or no input (Carpenter
 1979; FitzHugh 1955; Izhikevich 2007). Thresholds help to
 minimize noise propagation, which is critical for robustness
 in networks with multiple layers (Sarpeshkar 1998). Previous
 rate-based bipole models used an explicit rectification, or
 threshold, to prevent boundary propagation in response to
 individual inducers. In sLAMINART, such rectification is
 implicit and derives from Hodgkin-Huxley membrane
 dynamics within each cell.

Each cell's intracellular dynamics supports a graded, or
 analog, activation profile. A critical property of a properly
 designed network is that it retains analog sensitivity even as
 it binds multiple cell activations together into emergent
 groupings through recurrent interactions. Such a coexistence
 of analog sensitivity with coherent binding is called *analog
 coherence*, and helps to explain effects of contrast magnitude
 on perceptual grouping (Grossberg et al. 1997; Grossberg
 1999). sLAMINART successfully simulates a range of
 single-cell recording data about analog-sensitive perceptual
 grouping, and hereby shows how digital spiking dynamics
 can induce analog coherence. In particular, sLAMINART
 quantitatively simulates data about short-range grouping
 (Kapadia et al. 2000), long-range modulation (Crook et al.
 2002; Polat et al. 1998), contrast sensitivity (Polat et al.
 1998), horizontal summation (Chisum et al. 2003), and
 gamma-range oscillations (Gray et al. 1989). The next
 section describes the sLAMINART model, followed by a
 section that summarizes model simulations.

Table 2 Maximal bilateral extent of horizontal connections from selected studies

Species	Area	Horizontal extent [mm]	Selected references
Cat	Area 17	8	Gilbert and Wiesel (1983)
	Area 18	6.5 ^a	Kisvárdy et al. (1997)
Tree shrew	V1	8	Bosking et al. (1997)
Monkey	V1	7	Stetter et al. (2002)
	V2	8	Levitt et al. (1994)

^a Although the estimated horizontal extent appears smaller for area 18 than for area 17, the lower cortical magnification factor in area 18 (0.75 mm²/degrees² for area 18 Vs 3.6 mm²/degrees² for area 17 near area centralis; Tusa et al. 1979) means that horizontal connections in that area span a wider range of visual angle, and thus can be considered as functioning at a larger scale

493 **2 Method**

494 The sLAMINART model defines and simulates a layer 2/3
495 spiking bipole grouping circuit, fed by inputs from deeper
496 cortical layers, described for simplicity as layer 4 in Fig. 4.
497 Each spatial location along the horizontal axis roughly
498 corresponds to one hypercolumn. Pyramidal cells mutually
499 excite each other via long-range horizontal connections.
500 Inhibitory interneurons in each hypercolumn are divided
501 into two populations. As shown in Fig. 4, one population
502 receives excitatory long-range horizontal input from layer
503 2/3 pyramidal cells in hypercolumns located to their left.
504 The other population receives excitatory long-range hori-
505 zontal inputs from layer 2/3 pyramidal cells located to their
506 right. Henceforth we refer to the two populations of
507 interneurons as *Left* and *Right*, respectively. Each layer 2/3
508 inhibitory interneuron inhibits the layer 2/3 pyramidal cell
509 and the antagonist interneuron in the same hypercolumn.
510 This inhibitory scheme is designed to realize the bipole
511 property within a laminar cortical circuit (Grossberg and
512 Raizada 2000; Raizada and Grossberg 2001).

513 For example, when a pyramidal cell receives input from
514 a single excitatory pyramidal cell to its left, it also receives
515 a balanced inhibitory input from its Left inhibitory
516 interneuron (“one against one”). Hence, individual pyramidal
517 cells cannot cause run-away excitation across the network due
518 to the way in which the pyramidal cell temporally averages the
519 excitatory and inhibitory spikes. When a pyramidal cell
520 receives collinear inputs from excitatory pyramidal cells to
521 its left and its right, these flanking pyramidal cells activate the
522 corresponding Left and Right inhibitory interneurons. Both of
523 these interneurons inhibit the target pyramidal cell, as well as
524 one another. The mutual inhibition of the inhibitory interneur-
525 ons acts to normalize their total activity (Grossberg 1973). As
526 a result, the total excitation to the target pyramidal cell
527 increases, but the total inhibition remains similar to the level
528 of inhibition from an individual inhibitory interneuron (“two
529 against one”). The target pyramidal cell can therefore fire,
530 again due to the way in which the pyramidal cell temporally
531 averages the excitatory and inhibitory spikes.

532 Each layer of the model is composed of a one-
533 dimensional array of 51 neurons. Layer size is much larger
534 than the largest input stimulus simulated here (13 contigu-
535 ous spatial locations) in order to prevent boundary effects
536 which could have resulted from horizontal interactions.
537 Layer 4 cells are implemented with a single somatic
538 compartment governed by Hodgkin-Huxley dynamics.
539 External input to the model is provided via current injection
540 in the soma of layer 4 cells. Pyramidal cells and
541 interneurons in layer 2/3 have an additional passive
542 dendritic compartment, which is consistent with pyramidal
543 cell anatomy and enables smoother temporal integration of
544 excitatory inputs from other pyramidal cells. This smoother

integration results from the cable equation, whose leaky 545
integrator dynamics ensure that both the temporal integration 546
of inputs from pre-synaptic afferents into the dendritic 547
compartment, and the transfer of current from the dendrite to 548
the soma, are much slower than individual spike events. 549

Smooth integration is needed to obtain stable grouping 550
in the presence of pre-synaptic spikes that are not 551
coincident due to distance-dependent axonal delays and 552
the presence of noise. Besides providing better stability, the 553
presence of a dendritic compartment also allows selective 554
enhancement of inhibition by inhibitory synapses on the 555
soma, while excitatory synapses terminate on the dendrite 556
(Megías et al. 2001; Spruston 2008). This anatomy allows 557
inhibition to reach the soma faster than excitation, thereby 558
helping to prevent spurious outward propagation of activity. 559
Another consequence of this specific placement of synapses 560
is to make the spike trains of bipole cells look like that of 561
bursting cells, although they are not intrinsic bursters. 562
Indeed, the occurrence of an inhibitory spike to the soma of 563
an excited bipole cell is strong enough to induce a pause in 564
that cell’s otherwise constant firing activity, yielding spike 565
trains similar in appearance to various types of intrinsic 566
bursters (Carpenter 1979). 567

Synaptic interactions are implemented as double exponen- 568
tials with parameters corresponding to α -amino-3-hydroxy-5- 569
methylisoxazolepropionic acid (AMPA) and γ -amino-butyric 570
Acid (GABA) receptors for excitatory and inhibitory synap- 571
ses, respectively. The location of synaptic contacts is on the 572
passive dendrite for AMPAergic synapses and on the soma for 573
GABAergic synapses. The model includes realistic distance- 574
dependent axonal delays (Bringuier et al. 1999; Girard et al. 575
2001; Hirsch et al. 1991). Mathematical equations and 576 **Q8**
parameters, as well as details pertaining to the simulation 577
protocol, are included in the “Appendix”. All simulations 578
were conducted using *KDE Integrated Neurosimulation* 579
software (KInNeSS; Versace et al. 2008). 580

3 Results 581

3.1 Illusory contour 582

The combination of the above factors, notably the bipole- 583
organized balance of excitation and inhibition, intracellular 584
temporal spike averaging, and the differential locations of 585
excitatory and inhibitory contacts on soma and dendrite, 586
respectively, supports stable firing of layer 2/3 spiking 587
bipole cells during grouping of an illusory contour (Fig. 5). 588
The bottom plot of Fig. 5 shows a 1D stimulus pattern 589
corresponding to two collinear flanking stimuli (each 3 590
spatial locations wide) separated by a wide gap (5 spatial 591
locations). Inducers were simulated by injecting 0.03 nA 592
current inputs into layer 4 pyramidal cells. The middle plot 593

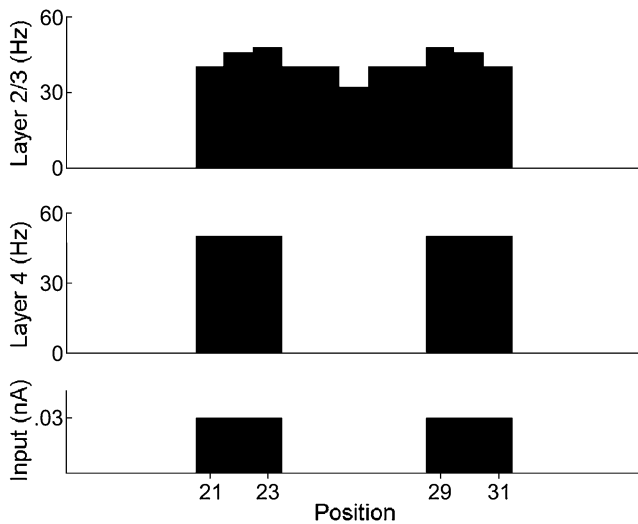


Fig. 5 Long-range completion in layer 2/3 spiking bipole cells: Two flanking stimuli (*bottom*) separated by a wide gap (5 hypercolumns) give rise to corresponding activity in layer 4 pyramidal cells (*middle*). The layer cell activities generate inputs activity pattern to vertically aligned layer 2/3 bipole cells (*top*), whose activation leads to inward completion of activity. Note the absence of outward propagation of activity. See text for further details

594 shows the firing rate of layer 4 pyramidal cells, where
 595 completion does not occur. Note, unless noted otherwise,
 596 reported firing rates are computed over 500 ms of
 597 simulation following an initial transient. The upper plot
 598 shows the firing rate of layer 2/3 bipole cells, where inward
 599 completion is present. Adding small amounts of noise in
 600 layer 2/3 dendrites leads to negligible activity in a few cells
 601 located just outside of the stimulus pattern.

602 **3.2 Short-range grouping**

603 Spatially short-range grouping is illustrated in Fig. 6, where
 604 model simulations are plotted together with monkey V1
 605 data from three different conditions: *flankers-only*, *target-*
 606 *only*, and *target-with-flankers* (Kapadia et al. 2000). The
 607 size of the illusory contour gap and of the inducers in these
 608 simulations was determined by taking into consideration
 609 the cortical magnification factor and details about the
 610 original experimental protocol. In particular, the gap and
 611 inducers both cover one spatial location in the simulations;
 612 see the “Appendix”. In the flankers-only condition, two
 613 bars were presented adjacent to the *classical receptive field*
 614 (CRF) of a recorded cell.

615 Note that the firing rate in the flankers-only grouping
 616 simulation of Fig. 5 is higher than that shown in Fig. 6.
 617 This is due to several interacting factors: First, the
 618 simulated illusory contour gap is wider in Fig. 5 than in
 619 Fig. 6, but the inducer length is also wider. Second, the
 620 horizontal projections are weaker than the bottom-up
 621 projections (in Table 3, g_{max} equals 0.003 and 0.049 for

horizontal and bottom-up projections, respectively). Thus, 622
 although the amount of current input in Fig. 5 was the same 623
 as in the high contrast conditions of Fig. 6 (0.03 nA in both 624
 cases, denoted as 50% contrast in Fig. 6), the amount of 625
 support is greater in Fig. 5, resulting in a higher firing rate 626
 in that case due to horizontal summation of wider bottom- 627
 up inputs. 628

The model explains the three cases depicted in Fig. 6 as 629
 follows. In the flankers-only condition, summation of 630
 horizontal inputs leads only to weak increments in firing 631
 rates, compared to the other two conditions, as noted above. 632
 Just as excitatory horizontal input is weak, inhibitory input 633
 to the target bipole is also weak, since interneurons in the 634
 target hypercolumn inhibit each other through recurrent 635
 connections. This balance of excitation and inhibition 636
 enables the target bipole to emit spike trains, resulting in 637
 short-range grouping. In the target-only condition, bottom- 638
 up input from the layer 4 cell activates the layer 2/3 bipole 639
 across a wide dynamic range. The reason why the range of 640
 firing rate is greater in this condition than in the other two is 641
 that it is the only one where inhibitory interneurons in the 642
 hypercolumn of the recorded bipole cell do not receive 643
 excitatory inputs from neighboring hypercolumns. Given 644
 the graded activity profile of single Hodgkin-Huxley cells 645
 modeled here (see Fig. 13 in the “Appendix”), the target 646
 bipole cell is thus free to span a wide range of firing rates. 647
 Finally, in the target-with-flankers condition, strong 648
 bottom-up input coupled with horizontal interactions results 649
 in a somewhat reduced dynamic range. The bottom-up and 650
 flanker inputs activate horizontal excitatory connections to 651
 all bipole cells in between. These recurrent excitatory 652

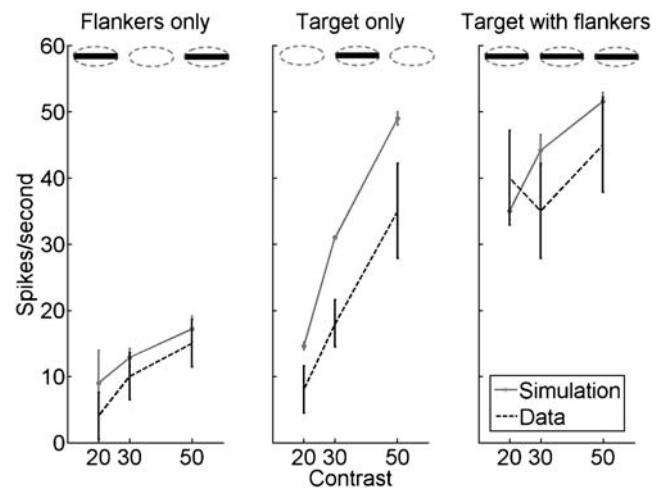


Fig. 6 Data from Kapadia et al. (2000) (dashed lines, reprinted with permission) and model simulations (solid lines). Error bars for the data represent variations among different cells/trials. Error bars for simulations represent variations among different parameter settings (see “Appendix”). The stimulus pattern in each case is indicated in the insets. See text for further details

Table 3 Synaptic connection parameters. Weights (W) and delays (δ_{Ax}) of horizontal connections are determined by Eqs. (13) and (14) respectively

	Pre-synaptic	Post-synaptic	Post-synaptic Site	E [mV]	g_{max} [mS/cm ²]	τ_r [ms]	τ_f [ms]	w	δ_{Ax} [ms]
t3.3	4 pyr.	2/3 pyr.	Dendrite	0	0.049	2	4	0.2	3
t3.4	2/3 pyr.	2/3 pyr.	Dendrite	0	0.003	2	6.5	–	–
t3.5	2/3 pyr.	2/3 int.	Dendrite	0	0.037	1	4	–	–
t3.6	2/3 int.	2/3 pyr.	Soma	–60	1.8	2	7	1	1
t3.7	2/3 int.	2/3 int.	Soma	–70	1	2	7	1	0.1

653 horizontal interactions cause a larger activation of the target
 654 cell even at low contrast. In addition, inhibitory interneurons
 655 in the target hypercolumn receive bilateral horizontal inputs.
 656 As a result, the interneurons inhibit each other through
 657 recurrent connections, as in the flankers-only condition. As
 658 contrast increases, the activity of the excitatory recurrent
 659 interactions and the inhibitory interneurons increases until the
 660 inhibitory interneuron activities reach the self-normalizing
 661 range, thereby helping to limit the increasing firing rate of the
 662 target bipole.

663 3.3 Long-range modulation: Two sides

664 At greater stimulus separations, contrast-dependent long-
 665 range modulation has been reported in pyramidal cells of
 666 area 17 (V1) in the cat (Polat et al. 1998). In that study, the
 667 activity of a target cell whose receptive field was stimulated
 668 with an optimally oriented bar was monitored in the absence
 669 or presence of flanking collinear stimuli. The stimulus bars
 670 were made long enough to cover the entire classical receptive
 671 field (CRF) of the recorded cell. In simulations, the bars span
 672 3 spatial locations. At low stimulus contrast, flanking inputs
 673 increased the activity of the target cell located between them,
 674 relative to when flankers are absent (facilitation condition),
 675 whereas at high stimulus contrast, they resulted in depression
 676 of activity relative to the no-flanker case. In the experiment,
 677 the separation between the flankers was determined by
 678 successively widening the gap until no grouping was
 679 observed. In the simulations, this occurred when the gap was
 680 widened to the point that it spanned 7 spatial locations,
 681 whereas grouping with gaps of width 5 and 1 have been
 682 obtained in Figs. 5 and 6, respectively. Figure 7 shows that
 683 the model simulates these data.

684 This result may be explained as follows: As in the target
 685 vs. target-with-flankers conditions of Fig. 6, target bipole
 686 firing is higher at low current input in the target-with-
 687 flankers. As current input to the target site increases, the
 688 inhibition on the target cell body from flanking interneurons
 689 limits the combined influence of bottom-up and horizontal
 690 excitatory inputs from further increasing target bipole activity.
 691 Figure 7 shows that, as current input increases, this limiting
 692 influence eventually results in greater target bipole activity in

the target-only condition than in the target-with-flankers
 condition. Such reversal of activity is not observed in the
 simulations of Fig. 6, where current input is not sufficiently
 high (the maximum current input is 0.03 nA in Fig. 6
 whereas it is 0.12 nA in Fig. 7).

3.4 Long-range modulation: One side

The bipole property can also enable one pyramidal cell to
 modulate the activity of a horizontally displaced cell, even
 though an individual pyramidal cell cannot cause signifi-
 cant suprathreshold grouping activity. Figure 8 reports
 simulation results and supporting evidence for this property
 from a cat V1 pyramidal cell (data from Crook et al. 2002).
 Unlike the previous experiments which employed pairs of

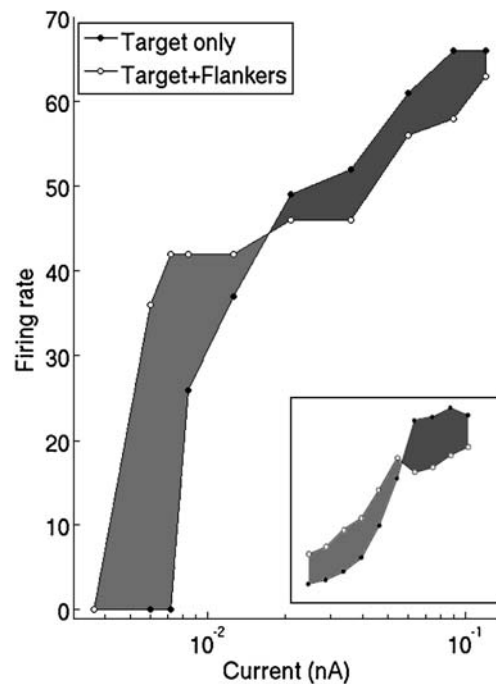


Fig. 7 Horizontal projections limit analog sensitivity over long distances. This is indicated by a flatter slope over most contrasts tested in the target-plus-flankers condition than in the target-only condition. The simulated activity can be compared to a sample result from Polat et al. (1998) shown in the inset. [Data reprinted with permission from Polat et al. (1998).]

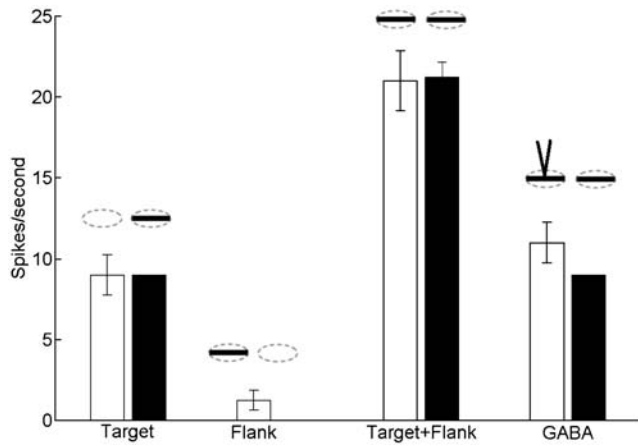


Fig. 8 Crook et al. (2002) neurophysiological data (*empty bars*) is matched with simulations (*dark bars*) in four conditions. Note the absence of outward propagation in the flanker-only condition. *Error bars* for the data represent the variation observed across different cells/trials, whereas they represent variations across different parameter settings for the simulations (see “Appendix”). [Data reprinted with permission from Crook et al. (2002).]

706 flankers, the data and simulations in Fig. 8 use a single
 707 flanker. In the *target-only* condition, a single optimally
 708 oriented bar was presented in the CRF of the target cell. In
 709 simulations, this bar length spans a single spatial location.
 710 In the *flanker-only* condition, a single collinearly oriented
 711 bar was presented in a location adjacent to the CRF of the
 712 cell. In the *target-with-flanker* condition, the target and
 713 flanker bars were presented simultaneously. The contrast of
 714 the flanker bar was 10 times higher than the contrast of the
 715 target bar. In simulations, current input to the target and
 716 flankers was 0.0096 nA and 0.06 nA, respectively, in order
 717 to approach this ratio. Finally, in the *GABA* condition, both
 718 the flanker and target bars were presented but with a
 719 simultaneous injection of GABA at the cortical activation
 720 site of the flanker stimulus.

721 As expected, cell activity was high in the *target-only*
 722 condition. In the model, this was due to bottom-up
 723 activation of the target layer 2/3 pyramidal cell. Activity
 724 of the target pyramidal cell was decreased to near zero in
 725 the *flanker-only* condition, reflecting the absence of
 726 outward completion from the flanker. In simulations,
 727 activity decreased to zero since, although flanker input to
 728 the target hypercolumn simultaneously excited the bipole
 729 cell and one inhibitory interneuron, the synaptic weights on
 730 the path leading to inhibition of the target bipole are
 731 stronger. Indeed, the maximal conductance g_{max} of layer 2/3
 732 horizontal projections between model pyramidal cells is
 733 0.003 μ S, whereas the maximal conductances for the
 734 pyramidal-to-interneuron and interneuron-to-pyramidal pro-
 735 jections are 0.037 μ S and 1.8 μ S, respectively (see Table 3).
 736 In comparison, in the flankers-only condition of Fig. 6,
 737 *bilateral* excitatory input caused the interneurons to inhibit

each other due to the recurrent connectivity, thereby leaving
 the bipole cell free to spike at a low level in that case.

Firing rates in Fig. 8 nearly doubled in the *target-with-*
flanker condition, relative to the target-only condition. As
 in Fig. 6, there is super-additive excitation in the target-
 with-flankers case. In Fig. 8, this is due to recurrent
 horizontal excitatory connections between the single flanker
 and the target cell, after bottom-up excitatory input from
 layer 4 to the target bipole cell allows it to overcome
 inhibition from the flanker site and to emit spikes. If GABA
 inhibits the flankers, then the target cell response returns
 to the level in the target-only condition.

3.5 Horizontal summation

The salience and strength of perceptual groupings depend
 upon the amount of *support* present in the image inducers
 (Leshner and Mingolla 1993; Soriano et al. 1996). Support is
 the ratio of the length of inducers to the total stimulus
 length. A correlate of this psychological observation is
 shown in physiological recordings of a layer 2/3 pyramidal
 cell in the tree shrew (Chisum et al. 2003). In this
 experiment, cell activity was monitored during presentation
 of stimulus bars of different lengths and at a predefined
 contrast level. Activation was reported as the ratio of firing
 activity obtained for the various stimulus lengths divided by
 the activity obtained for a wider bar of higher contrast.
 Figure 9 shows model bipole cell activity as a function of

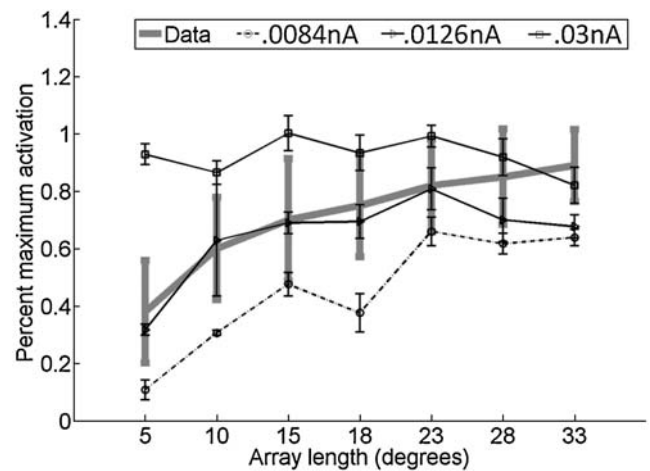


Fig. 9 Activity of a layer 2/3 cell in area V1 of a tree shrew (*continuous thick curve*) is shown here as the ratio of activity (firing rate) obtained at a particular inducer length with respect to the activity in response to a longer stimulus at high contrast. In the simulations, this baseline stimulus spans 13 hypercolumns and corresponds to a current input of 0.0408 nA. Horizontal summation in the data is consistent with model simulations at lower current inputs (0.0084 and 0.0126 nA), whereas saturation is observed at the high current input simulated (0.03 nA). *Error bars* in the data represent variations across different cells/trials. They represent variation across different parameters (see “Appendix”) in the simulations. [Data reprinted with permission from Chisum et al. (2003).]

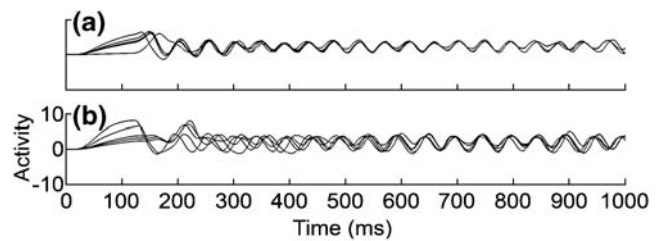
764 the length (in degrees of visual angle) of the stimulus
 765 presented at different contrast levels (the contrast levels
 766 tested correspond to current inputs of 0.0084, 0.0126 and
 767 0.03 nA) and overlaid on a subset of the Chisum et al.
 768 (2003) data. Horizontal summation is indicated by the fact
 769 that, as the array width gradually increases from one spatial
 770 location to seven, relative activity with respect to a long
 771 high contrast stimulus bar (13 spatial locations wide,
 772 current input of 0.048 nA), tends toward 1. See the
 773 “Appendix” for details on how the degrees of visual angle
 774 from the experimental study were matched to the number of
 775 locations spanned in present simulations.

776 This result may be explained by noting that the target
 777 bipole cell receives excitatory input from a progressively
 778 larger number of flanking bipole cells as the stimulus bar
 779 gets wider. At low contrast, excitation from horizontal
 780 projections is slightly stronger than inhibition, which results
 781 in an increase in target bipole firing rate as a function of
 782 inducer length. However, at the highest level of contrast
 783 tested, the influence of inhibition becomes more pro-
 784 nounced, such that further increasing the inducer length
 785 does not increase the activity of the target bipole. Note in
 786 particular how the relative activity plotted for this contrast
 787 level approximates 1, meaning that it approaches the
 788 activity obtained in the case of the 13-units wide bar at
 789 even higher contrast. The model thus predicts that horizon-
 790 tal summation exerts a significant effect at lower contrasts
 791 but less so at high contrast. This is compatible with the
 792 simulations of short-range grouping of Fig. 6 and long-
 793 range modulation of Fig. 7, where the impact of inhibition
 794 on the target bipole cell is accentuated at similarly high
 795 contrast levels (i.e., for current inputs of 0.03 nA), resulting
 796 in a reduction in analog sensitivity.

797 3.6 Gamma band oscillations, synchrony and perceptual
 798 grouping

799 A number of investigators have reported synchronous oscil-
 800 lations during perceptual grouping, among other brain
 801 processes; e.g., Eckhorn et al. (1988) and Gray et al. (1989).
 802 Bipole grouping in rate-based models is capable of fast
 803 synchronization of boundary groupings, including illusory
 804 contours and fast resynchronization after inputs change.
 805 Synchronization occurs both in non-laminar models (Gross-
 806 berg and Grunewald 1997; Grossberg and Somers 1991) and
 807 laminar cortical models (Yazdanbakhsh and Grossberg 2004).

808 To study whether and how resynchronization occurs in
 809 the spiking laminar cortical sLAMINART model, simula-
 810 tions were conducted by presenting a random pattern of
 811 activation for the first 100 ms, thereby randomizing the
 812 firing phases of layer 2/3 pyramidal cells, and then
 813 switching to either a real contour (Fig. 10(a)) or an illusory
 814 contour (Fig. 10(b)). The resulting layer 2/3 membrane



815 **Fig. 10** (a) Fast resynchronization of bursts in the presence of a real
 816 contour. A random pattern was presented for the first 100 ms and
 817 followed by a static real boundary contour stimulus. Oscillations
 818 shown here correspond to the middle 5 units along the contour, which
 819 was 9 units wide. (b) Slower resynchronization of bursts in the
 820 presence of an illusory contour. The gap between inducers was 3 units

815 potential traces were then low-pass filtered to preserve only
 816 burst oscillations. This is consistent with the observation
 817 that the oscillations found in the study of Gray et al. (1989)
 818 were mostly due to bursts, rather than to single-spike
 819 coincidence. Figure 10(a) shows resynchronization occurring
 820 in the 100 ms following input change. Figure 10(b) shows
 821 resynchronization to occur around 300 ms later. The faster
 822 synchronization observed for real contours is due to the fact
 823 that layer 4 activity, which drives the activity of layer 2/3, is
 824 synchronous along the simulated contour. This result is
 825 consistent with data showing that illusory contours take
 826 longer to be perceived than real contours (Francis et al. 1994;
 827 Meyer and Ming 1988).

828 During synchronization, the bipole grouping network
 829 exhibits oscillatory synchrony in the low gamma range
 830 (>20 Hz) along a grouped contour (Fig. 11), a claim supported
 831 by a wide range of electrophysiological evidence (e.g. Gray
 832 et al. 1989; Samonds et al. 2006). This result is related to,
 833 but differs in an important way, from the *binding-by-*
 834 *synchrony* hypothesis (Milner 1974; von der Malsburg
 835 1981). In the sLAMINART model, it is more proper to
 836 describe a *synchrony-by-binding* hypothesis, since synchro-
 837 nization, when it occurs at all in a bipole network, is an
 838 emergent property of how recurrent network interactions
 839 bind cells together during perceptual grouping. According to
 840 the experimental study of Gray et al. (1989), phase locking
 841 between a pair of pyramidal neurons is strongest in area 17
 842 of the cat when a single contour spans the collinear CRF of
 843 the two recorded cells (Fig. 11, upper left row). Synchrony is
 844 reduced at locations on an illusory contour (middle left row),
 845 and is non-existent during presentation of uncorrelated
 846 moving bars (bottom left row). Simulations (middle column)
 847 agree qualitatively with the empirical cross-correlograms.

848 The single contour condition was simulated as a single
 849 inducer, 11 spatial locations wide. For the illusory contour
 850 condition, inducer bar and gap length were set to 3 and 5
 851 spatial locations, respectively, as in Fig. 5. The uncorrelated
 852 bars were simulated by alternately presenting each inducer
 853 from the illusory contour condition. Inducers were simu-

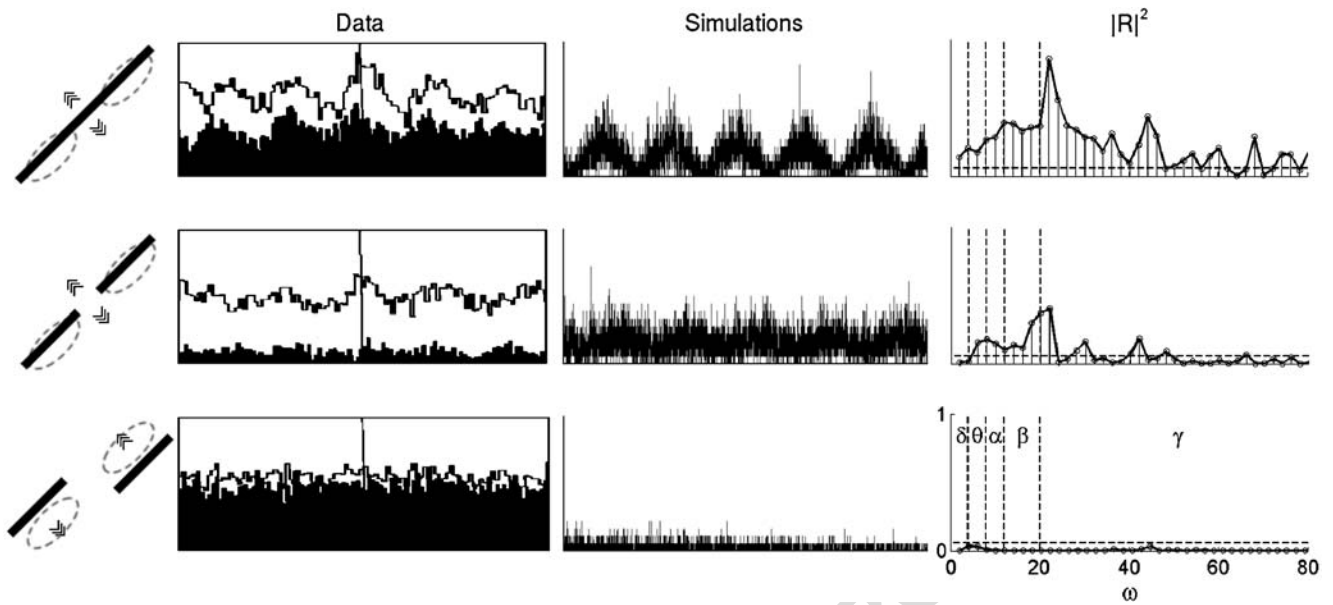


Fig. 11 (Left) Data of Gray et al. (1989) showing that synchrony between pyramidal cells in cat area 17 is strongest for a continuous bar stimulus, weaker at an illusory contour induced by a part of collinear bars, and absent between non-collinear bars. (Middle) Model simulations replicate these data. (Right) The synchronous coupling

in the model is statistically significant at a confidence level of 5% in the full bar and coherent bar cases and absent in the incoherent bar case, as indicated by the coherence index $|R|^2$. [Data reprinted with permission from Gray et al. (1989)]

854 lated by injecting 0.03 nA current input. A phase
855 randomizing signal was further included by injecting time-
856 varying noise of amplitude up to 0.003 nA in the dendrite
857 of layer 2/3 pyramidal cells.

858 The exact nature of synchronous oscillations in the
859 simulated spike trains is further probed in the right column,
860 where points above the horizontal dashed line indicate
861 significant coherence at a particular frequency (cf. Rosenberg
862 et al. 1989). This analysis confirms the presence of low-
863 range gamma oscillations (20–40 Hz) along boundary
864 groupings. Comparison of the single contour and illusory
865 contour conditions reveals that phase-locked layer 4 activity
866 transmitted via layer 2/3 bipole cells located within a pair of
867 nearby layer 2/3 bipoles helps to synchronize activity along
868 the represented contour. This is to be expected from the
869 symmetry of the bipole kernel: bipoles located in the middle
870 project equally strongly to bipoles on the left and right of the
871 contour (see Golubitsky and Stewart (2006) for a discussion
872 of synchrony-inducing symmetry). The spectral analysis in
873 the right column further shows that the shape of the
874 frequency spectrum remains roughly similar across the two
875 conditions. The main difference resides in the magnitude of
876 the spectrum in each frequency bin, which again reflects the
877 influence of excitation and inhibition from bipole cells in the
878 middle. In other words, both real and illusory contours
879 produce oscillations mainly in the gamma range, but illusory
880 contours display less power overall. However, oscillatory
881 synchrony in this condition remains stronger than in the
882 alternating contour condition, where horizontal excitatory

883 signals from one side of the contour are insufficient to trigger
884 reliable spiking in bipoles on the other side in the absence of
885 concurrent bottom-up input.

886 The gamma oscillations depicted in Fig. 11 remain when
887 measured at a larger scale. In the experimental literature,
888 gamma synchronization of evoked potentials has been
889 found during viewing of grouping stimuli. In particular,
890 Tallon et al. (1995) reported a 30 Hz component over areas
891 covering visual cortices in response to a Kanizsa triangle
892 stimulus. In order to probe the synchronous dynamics of
893 the network measured at a larger scale, cell activity across
894 the 1D array of layer 2/3 cells obtained during simulations
895 of an illusory contour (8 units wide flankers separated by a
896 5 units wide gap) was combined into a single estimate of
897 the local field potential (LFP) according to the methodol-
898 ogy described in Versace et al. (2008). The resulting signal
899 was Fourier transformed (FFT) to obtain the power
900 spectrum displayed in Fig. 12. This result suggests that
901 the large-scale gamma oscillations observed in response to
902 grouping stimuli may either originate in the bipole circuit,
903 or at least be partially supported by it.

4 Discussion

4.1 Summary of findings

This article demonstrates for the first time how a network of layer 2/3 recurrently interacting spiking neurons with

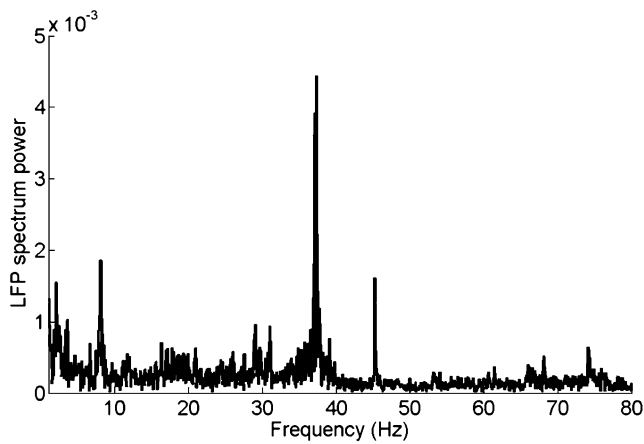


Fig. 12 Local field potential (LFP) spectrum power in model layer 2/3. A clear peak is observed in the low gamma range. This result reflects the pattern of LFP spectrum power obtained using various stimulus configurations. See text for details

908 multiple compartments that obey Hodgkin-Huxley dynamics
 909 may perform stable, analog coherent, and synchronous
 910 perceptual grouping of both real and illusory contours in a
 911 manner that quantitatively reproduces key neurophysiological
 912 data from multiple laboratories. This sLAMINART model
 913 shows how recurrent intralaminar feedback within layer 2/3
 914 responds to initial feedforward activation upon presentation of
 915 a grouping stimulus in order to complete a stable boundary
 916 representation. Whereas spiking dynamics have in various
 917 other models been implemented using highly simplified
 918 mechanisms (e.g., integrate-and-fire dynamics in a single
 919 dimensionless compartment), the sLAMINART model is
 920 defined by more realistic brain mechanisms, including
 921 Hodgkin-Huxley cell dynamics, multiple cellular compart-
 922 ments, excitatory and inhibitory recurrent interactions that
 923 terminate on cell dendrites and somata, respectively, and
 924 distance-dependent axonal delays. In addition, the selective
 925 grouping properties that exemplify the bipole property are
 926 realized without the use of explicit thresholds, since the latter
 927 are implicitly included in Hodgkin-Huxley dynamics for the
 928 combination of parameters used here.

929 The emergence of stable grouping despite the presence
 930 of distant-dependent axonal delays and the addition of noise
 931 in our simulations demonstrates that perfect coincidence in
 932 spike timing is not necessary for grouping to occur. Rather,
 933 an instantaneous spike event exerts a temporally persistent
 934 influence on bipole cells principally due to the time course
 935 of EPSPs and IPSPs (see Appendix Eq. (10)), and of inter-
 936 compartmental currents. These slower processes allow for
 937 temporal summation of multiple presynaptic spike trains,
 938 thereby enabling the network dynamics as a whole to
 939 exhibit properties like analog coherence and sensitivity to
 940 the extent of stimulus support.

941 The differential localization of excitatory and inhibitory
 942 terminals on bipole cells, with excitatory synapses on the

dendrites and inhibitory synapses on the soma, means that 943
 inhibition can act much faster on the soma than excitation 944
 does, thereby preventing the unwanted outward propagation 945
 of signals outside of the inducers' locations. This is further 946
 guaranteed by the larger conductance of inhibitory synapses 947
 than excitatory synapses in the model. 948

The balance of inhibition and excitation is critical to 949
 explain the data on long-range modulation (Fig. 7). These 950
 data were also simulated in a previous non-spiking laminar 951
 cortical model of perceptual grouping by Grossberg and 952
 Raizada (2000). That simulation required modulatory 953
 feedback from V2 bipole cells to the V1 network. The 954
 current study shows how a properly balanced network of 955
 spiking layer 2/3 cells within V1 is sufficient to generate 956
 this result. 957

The simulations of fast synchronization highlight the 958
 relationship between boundary grouping and gamma 959
 oscillations that has been reported in the neurophysiological 960
 literature (e.g. Gray et al. 1989; Gray and Singer 1989; 961
 Samonds et al. 2006). Gamma oscillations have also been 962
 shown to occur in model simulations when a sufficiently 963
 good match occurs between bottom-up feature patterns and 964
 top-down attentive learned expectations during attentive 965
 category learning and recognition (Grossberg and Versace 966
 2008), thereby providing a mechanistic explanation of how 967
 gamma oscillations can occur during attentive states (Fries 968
 et al. 2001; Gregoriou et al. 2009). These two examples 969
 show that gamma synchronization can be the result of quite 970
 different brain mechanisms. 971

These results also argue against a binding-by-synchrony 972
 hypothesis. Rather, they illustrate how gamma synchroni- 973
 zation may result as an emergent property of functionally 974
 distinct types of "binding". Moreover, synchronization need 975
 not occur only in the gamma frequency range, even in the 976
 same brain network. It may occur in different frequency 977
 ranges within the same network due to task constraints. 978
 Grossberg and Versace (2008) have predicted, for example, 979
 that slower beta oscillations can occur when a mismatch 980
 occurs between bottom-up and top-down signal patterns, 981
 and at least three laboratories have reported data that are 982
 consistent with this prediction (Berke et al. 2008; Buffalo et 983
 al. 2004; Buschman and Miller 2008). Grossberg and 984
 Versace (2008) have also predicted why more beta 985
 oscillations may be found in the deeper layers of visual 986
 cortex, as reported by Buffalo et al. (2004), and Grossberg 987
 (2009) has proposed an explanation of why beta oscil- 988
 lations occur in the hippocampal place cell learning data of 989
 Berke et al. (2008). 990

4.2 Comparison with other spiking models of grouping 991

The fact that exact coincidence of spikes is not required in 992
 order to represent boundary contours in the model (cf. 993

994 Fig. 10) illustrates that the grouping mechanism is robust.
 995 A related mechanism of asynchronous spike-based contour
 996 completion—employing long-range anisotropic excitatory
 997 connections, but lacking inhibitory interneurons—was
 998 proposed in VanRullen et al. (2001). Runaway excitation
 999 in the model was prevented by artificially limiting each
 1000 neuron to emit no more than one spike. Simulations showed
 1001 that their network can account for cooperation among
 1002 neighboring collinear inducers (i.e., it can perform contour
 1003 integration). However, the authors did not test necessary
 1004 computational properties such as the bipole property,
 1005 stability of the emergent grouping over time, analog
 1006 sensitivity, and horizontal summation. In particular, contour
 1007 persistence is not addressed due to the constraint of a single
 1008 spike per neuron. Illusory contours are assumed completed
 1009 as soon as neurons on top of the gap spike once. Since this
 1010 occurs as a result of fast feedforward accumulation of single
 1011 spikes from collinear neighbors that receive bottom-up
 1012 input, it is not clear how much asynchrony the network can
 1013 tolerate. Another consequence of the emphasis on fast
 1014 feedforward integration is that the model predicts that real
 1015 and illusory contours take approximately the same amount
 1016 of time to be perceived, which is inconsistent with
 1017 psychophysical data.

1018 Yen et al. (1999) simulated a more elaborate network of
 1019 compartmental neurons in which a kernel of long-range
 1020 anisotropic excitatory connections was used to promote
 1021 synchronous spiking among populations coding for collinear
 1022 edges, with the intent of showing how spike timing could be
 1023 used as an index of which edge a given neuron represents.
 1024 However, the stimuli used in that study consisted only of real
 1025 boundary contours. It is not clear whether the network could
 1026 perform boundary completion, notably illusory contour
 1027 completion. In addition, the authors did not test for the
 1028 presence of spurious outward propagation and did not
 1029 address the requirement of analog coherence.

1030 Yen and Finkel (1998) proposed a model of contour
 1031 grouping based on synchronization of neural oscillators.
 1032 However, suprathreshold activation of a cell required direct
 1033 bottom-up input, implying that their model could not
 1034 do boundary completion, notably formation of illusory
 1035 contours. Moreover, in our model, gamma oscillations are
 1036 an emergent property of cells which, left alone, do not
 1037 oscillate.

1038 Domijan et al. (2007) implemented a one-dimensional
 1039 network of non-spiking compartmental bipole cells based
 1040 on the original Boundary Contour System model of
 1041 Grossberg and Mingolla (1985a). The dendritic tree of
 1042 bipole cells in the model was restricted to two branches:
 1043 one that collects horizontal inputs from the left and the
 1044 other one from the right. Their simulations replicated the
 1045 bipole property, analog sensitivity, and horizontal summa-
 1046 tion. The crucial mechanism consisted in the explicit

1047 multiplication of the contribution of both dendritic branches
 1048 (an AND-gate that preserves analog sensitivity). The model
 1049 therefore embodies the following two assumptions: (1) the
 1050 presence of multiplicative interactions between separate
 1051 dendritic branches, and (2) the anisotropic distribution of
 1052 postsynaptic sites on the dendrite tree, as dictated by the
 1053 location of the presynaptic cell (i.e., pre-synaptic inputs
 1054 from the left target the dendrite on the left, and vice-versa).
 1055 The first assumption is contradicted by recent experimental
 1056 findings that supralinear summation occurs only between
 1057 synaptic sites on a single branch, whereas inputs from
 1058 different branches sum only linearly (Polsky et al. 2004).
 1059 The second assumption would be supported if the shape of
 1060 dendritic trees were anisotropic. However, anatomical
 1061 evidence suggests that dendritic trees, at least in layer 3 of
 1062 visual cortices, are isotropic (Elston et al. 1996). Thus it
 1063 remains to be shown how such an anisotropic distribution
 1064 of synaptic inputs on isotropic dendritic trees could result
 1065 from experience-induced development. This model does
 1066 not incorporate spiking dynamics nor conduction delays,
 1067 and does not strictly implement the cable equation (e.g.,
 1068 there are no bidirectional interactions between compart-
 1069 ments and temporal integration is not present in the
 1070 dendrites). In other words, the model does not address the
 1071 problem of how neurons integrate asynchronous spikes to
 1072 achieve perceptual grouping. Thus, this model does not
 1073 incorporate several neurophysiological constraints that
 1074 support sLAMINART quantitative simulations of key
 1075 neurophysiological data.

5 Conclusion

1076
 1077 The sLAMINART model shows how networks of spiking
 1078 cortical cells in layer 2/3 group collinear contour fragments
 1079 into unified boundary contours. In particular, simulations
 1080 show that the model is able to realize the bipole property,
 1081 and in doing so, achieves good qualitative and sometimes
 1082 quantitative agreement with a range of previously published
 1083 single-cell data about grouping. Perceptual grouping in
 1084 sLAMINART is temporally stable, is accompanied by
 1085 oscillatory synchrony in the gamma range along a grouped
 1086 contour, and is sensitive to both the contrast and length of
 1087 contour inducers, thereby realizing the property of analog
 1088 coherence in a network of spiking neurons.

Appendix

Model

1090
 1091 First the mathematical equations for single cell dynamics
 1092 are described, followed by network equations.

1093 Hodgkin-Huxley dynamics and compartmental equations
 1094 Neurons are implemented as either one or two compartments
 1095 governed by cable equations (Segev 1998). Compartmental
 1096 membrane potential V is governed by an equation of the
 1097 form:

$$C_m \frac{dV}{dt} = - \sum_k I_k, \tag{1}$$

1098 where I_k refers to either of synaptic, axial, injected or
 1100 membrane channel currents, as explained below. Membrane
 1101 capacitance C_m is a function of compartment diameter (d)
 1102 and length (l), and specific capacitance C_M :

$$C_m = \pi d l C_M. \tag{2}$$

1103 In accordance with general practice, we set $C_M =$
 1106 $1 \mu\text{F}/\text{cm}^2$ (Koch 1999). Compartment dimensions d and
 1107 l are the same for all neurons of a given layer. For clarity,
 1108 dV/dt is noted dS/dt when the compartment is the soma,
 1109 and by dD/dt when the compartment is a dendrite.

1110 Somatic compartments are governed in part by Hodgkin-
 1111 Huxley (1952) equations. To simplify notation, the collec-
 1112 tive influence of the leak, K^+ , and Na^+ currents is denoted
 1113 $f(S_i^j)$, where S_i^j stands for the somatic membrane potential
 1114 of unit i in layer j :

$$f(S_i^j) = -g_L(S_i^j + |E_L|) - g_K n^4(S_i^j + |E_K|) + g_{Na} m^3 h(E_{Na} - S_i^j), \tag{3}$$

1116 where g_L , g_K and g_{Na} are the maximal conductances of the
 1117 leak, K^+ , and Na^+ channels respectively. E_L , E_K and E_{Na}
 1118 represent the reverse potentials of the three respective
 1119 currents, with specific values shown in Tables 3 and 4. The
 1120 short form in (3) is not used for dendritic compartments
 1121 since, for simplicity, the latter only have a passive leak
 1122 current term $g_L(D_i^j + |E_L|)$. Gate variables n , m and h stand
 1123 for the K^+ and Na^+ activating gates, and the Na^+
 1124 deactivating gate, respectively. The dynamical behavior of

these gates is governed by the differential equation (where
 $k = \{n, m, h\}$):

$$\frac{dk}{dt} = \alpha_k(S_i^j)(1 - k) - \beta_k(S_i^j k). \tag{4}$$

The rate functions $\alpha_k(S_i^j)$ and $\beta_k(S_i^j)$ for the n , m and
 h gating variables are given in Eqs. (5)–(7), respectively. The
 parameters for these equations were adapted from Traub and
 Miles (1991) such that cells transition to spiking through a
 supercritical Andronov-Hopf bifurcation (Izhikevich 2007)
 and have a stable attractor for small external input:

$$\alpha_n(V) = 0.032 \frac{15-V}{\exp(\frac{15-V}{5})-1} \tag{5}$$

$$\beta_n(V) = 0.5 \exp(\frac{-13.7-V}{40}),$$

$$\alpha_m(V) = 0.32 \frac{13.0-V}{\exp(\frac{13-V}{4})-1} \tag{6}$$

$$\beta_m(V) = -0.28 \frac{40-V}{\exp(\frac{40-V}{-5})-1},$$

and

$$\alpha_h = 0.128 \exp(\frac{17-V}{18}) \tag{7}$$

$$\beta_h = \frac{4}{\exp(\frac{40-V}{5})+1}.$$

Setting $n(t) + h(t) \approx 0.84$ and $m = m_\infty(V)$, the (V, n) -
 phase plane (Izhikevich 2007) resulting from this choice of
 parameters is shown in Fig. 13. It can be seen that, with
 these parameters, model neurons behave as threshold units,
 firing only for sufficiently depolarizing input.

For inter-compartmental currents, the *actual* axial con-
 ductance of neurons within layer j is denoted q_j^c and is
 defined by:

$$q_j^c = \frac{\pi d_j^c{}^2}{4 l_j^c R_j^A}. \tag{8}$$

Note that the diameter d_j^c and length l_j^c are the
 dimensions of the compartment c towards which the current
 appears to be directed in the relevant equation. Thus, c is

t4.1 **Table 4** Cell compartment dimensions, passive leak and axial conductivity parameters

t4.2	Population	Compartment	Diameter [mm]	Length [mm]	g_{leak} [mS/cm ²]	E_{leak} [mV]	Axial resistance [K·Ωcm]
t4.3	4 pyr.	Soma	0.001	0.005	0.01	-60	-
t4.4	2/3 pyr.	Soma	0.001	0.012	0.001	-60	-
t4.5		Dendrite	0.001	0.032	0.005	-60	10
t4.6	2/3 int.	Soma	0.001	0.01	0.01	-60	-
t4.7		Dendrite	0.001	0.007	0.005	-60	10

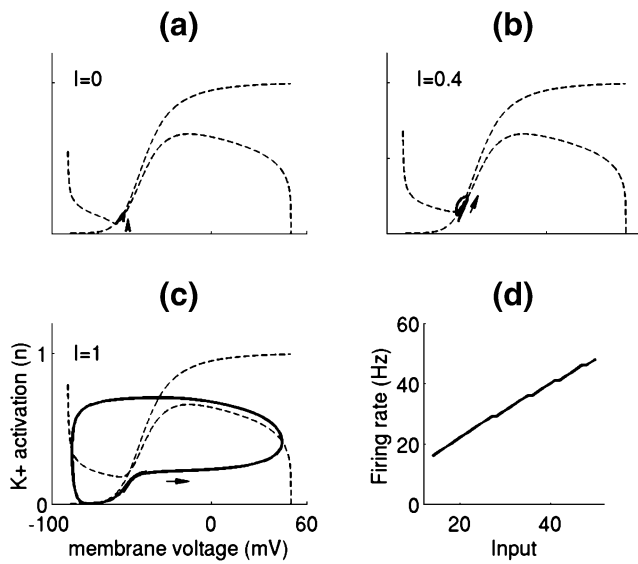


Fig. 13 (a)–(c) Parameters used for Hodgkin-Huxley equations allow model neurons to lose stability through a supercritical Andronov-Hopf bifurcation with increasing current input strength (I). The presence of a stable attractor at low I ensures limited outward propagation of signals in the bipole network. (d) These settings also render model neurons analog sensitive in terms of firing rate (Hz)

1155 replaced by S in the case of the soma and by D in the case
 1156 of dendrite. Parameter R_j^A denotes specific axial resistance
 1157 for neurons in layer j .
 1158 Synaptic input I_{ij}^{kl} from unit i of layer k to unit j of layer
 1159 l is modeled by:

$$I_{ij}^{kl} = w_{ij}^{kl} \left(\sum_{t_n \in S_{ij}^{kl}} g_{ij}^{kl}(t - \delta_{ij}^{kl}, t_n) - \prod_{t_n \in S_{ij}^{kl}} g_{ij}^{kl}(t - \delta_{ij}^{kl}, t_n) \right), \quad (9)$$

1160 where δ_{ij}^{kl} stands for axonal delay for that particular synaptic
 1162 connection. Function $g_{ij}^{kl}(t - \delta_{ij}^{kl}, t_n)$ is a double exponential
 1163 tail (e.g. Köhn and Wörgötter 1998):

$$g_{ij}^{kl}(t - \delta_{ij}^{kl}, t_n) = \begin{cases} \frac{p}{\tau_f - \tau_r} \left(e^{-\frac{t - \delta_{ij}^{kl} - t_n}{\tau_f}} - e^{-\frac{t - \delta_{ij}^{kl} - t_n}{\tau_r}} \right) & \tau_r \neq \tau_f \\ \frac{t}{\tau_r} e^{1 - \frac{t - \delta_{ij}^{kl} - t_n}{\tau_r}} & \tau_r = \tau_f \end{cases}. \quad (10)$$

1166 Constants τ_r and τ_f represent the rise-time and fall-time,
 1167 respectively, of $g_{ij}^{kl}(t - \delta_{ij}^{kl}, t_n)$, which closely determines
 1168 excitatory and inhibitory postsynaptic potentials (EPSP/
 1169 IPSP) shape and duration (see Table 3). Constant p is set to
 1170 ensure that $g_{ij}^{kl}(\cdot) \in [0, 1]$. The summation and multiplication
 1171 in (9) are taken over the set S_{ij}^{kl} of the last two spike
 1172 times t_n from unit i of layer k to unit j of layer l . Thus,

keeping in mind that $g_{ij}^{kl}(\cdot) \in [0, 1]$, the multiplicative term
 1173 ensures that the aggregated conductances remain between 0
 1174 and 1, which implies that synaptic current I_{ij}^{kl} varies
 1175 between 0 and w_{ij}^{kl} . In the case of one-to-one connections,
 1176 such that $i=j$, we abbreviate I_{ij}^{kl} by I_i^{kl} in Eq. (9).
 1177

The synaptic current resulting from the use of Eq. (9) is
 1178 obtained by multiplying I_{ij}^{kl} with the voltage difference
 1179 $(E - V_j^l)$. Here, V_j^l is the membrane voltage of the post-
 1180 synaptic compartment of cell j in layer l , and E is the
 1181 driving potential specific to the type of synapse under
 1182 consideration. For excitatory connections, E is set to a
 1183 depolarizing value (0 mV). For inhibitory connections, E is
 1184 set to a hyperpolarizing value (−60 or −70 mV).
 1185

Network equations 1186

The neural network is composed of 1-dimensional arrays of
 1187 layer 4 and layer 2/3 pyramidal cells and *Left* and *Right*
 1188 interneurons. Each of the four layers contains 51 neurons.
 1189 Figure 2 illustrates a representative diagram of the network
 1190 where layer 2/3 cells and interneurons span 7 spatial
 1191 locations. External input is provided at each layer 4
 1192 pyramidal cell. Each layer 4 cell projects to a single layer
 1193 2/3 cell. Horizontal excitatory connections originating from
 1194 layer 2/3 cell span a total of 7 spatial locations. *Left*
 1195 interneurons receive such horizontal connections only from
 1196 layer 2/3 cells on their left. The reverse holds for *Right*
 1197 interneurons. *Left* and *Right* interneurons at a given spatial
 1198 location inhibit each other via recurrent connections. Both
 1199 interneurons also inhibit the layer 2/3 cell at the same
 1200 spatial location. These connections are described more
 1201 precisely below.
 1202

All network equations are written with endogenous
 1203 currents (ionic channels, inter-compartmental) on the left-
 1204 hand side and exogenous currents (synaptic, injections) on
 1205 the right-hand side.
 1206

Layer 4 pyramidal cells 1207

Each layer 4 pyramidal cell is modeled as a single
 1208 compartment (a soma) S_i^4 that receives externally injected
 1209 input X_i , where the latter is a scalar value for each neuron
 1210 that is determined according to the simulation (see below):
 1211

$$C_m \frac{dS_i^4}{dt} - f(S_i^4) = X_i. \quad (11)$$

Layer 2/3 pyramidal cells 1214

Each layer 2/3 pyramidal cell is composed of one soma (S_i^2)
 1215 and one dendrite (D_i^2) compartment. The dendritic com-
 1216

1217 partment receives bottom-up excitatory input from one
 1218 layer 4 pyramidal cell (I_i^{42}) and recurrent excitatory input
 1219 from a Gaussian neighborhood of layer 2/3 pyramidal
 1220 cells ($\sum_{m=i-3}^{i+3} I_{mi}^{22}$):

$$C_m \frac{dD_i^2}{dt} - q_2^D (S_i^2 - D_i^2) + g_L (D_i^2 + |E_L|) = (E_{AMPA} - D_i^2) I_i^{42} + (E_{AMPA} - D_i^2) \sum_{m=i-3}^{i+3} I_{mi}^{22}. \quad (12)$$

1223 The Gaussian distributed weight kernel and the axonal
 1224 delay kernel implicit in I_{mi}^{22} are determined by Eqs. (13) and
 1225 (14), respectively:

$$w_{mi}^{kl} = g_{\max} e^{-(m-i)^2/\sigma^2}, \quad (13)$$

1226

$$\delta_{mi}^{kl} = 1 + 3 \cdot |i - m|, \quad (14)$$

1230 where m and i are the indices of the pre- and post- synaptic
 1231 units respectively, and $\sigma = 4.47$. The maximal conductance,
 1232 g_{\max} , is specific to the projection and values used for it are
 1233 in Table 3.

1234 The somatic potential is defined as follows: Input from
 1235 layer 2/3 pyramidal cells is significantly delayed in time,
 1236 reflecting the presence of slow conduction delays in layer 2/3
 1237 horizontal connections. The soma receives convergent inhib-
 1238 itory input from the *Left* and *Right* interneurons at the same
 1239 spatial location ($I_i^{L2} + I_i^{R2}$):

$$C_m \frac{dS_i^2}{dt} - q_2^S (D_i^2 - S_i^2) - f(S_i^2) = -(S_i^2 + |E_{GABA}|) [I_i^{L2} + I_i^{R2}]. \quad (15)$$

1240 Equation (15) implies that inhibitory interneurons have a
 1243 decisive effect on the layer 2/3 pyramidal cell they
 1244 innervate due to their direct action on the soma.

1245 Layer 2/3 inhibitory interneurons

1246 Layer 2/3 interneurons are divided into two groups
 1247 according to whether they are to the *Left* or to the *Right*
 1248 of the layer 2/3 pyramidal cell they innervate. Since the
 1249 form of the differential equations is similar and all
 1250 parameters are the same, only equations for *Left* interneu-
 1251 rons are explicitly given here. Each *Left* layer 2/3 interneu-
 1252 ron is composed of one soma (S_i^L) and one dendrite (D_i^L)
 1253 compartment. The dendritic compartment receives excitatory

input from a half-Gaussian neighborhood of Layer 2/3
 pyramidal cells located to its left ($\sum_{m=i-3}^{i-1} I_{mi}^{2L}$):

$$C_m \frac{dD_i^L}{dt} - q_L^D (S_i^L - D_i^L) + g_L (D_i^L + |E_L|) = (E_{AMPA} - D_i^L) \sum_{m=i-3}^{i-1} I_{mi}^{2L}. \quad (16)$$

The synaptic weight and axonal delay parameters that
 define I_{mi}^{2L} are determined by Eqs. (13) and (14), respec-
 tively, with the additional constraint that it is set to 0 for
 $m > i$ in the case of *Left* interneurons and for $m < i$ in the
 case of *Right* interneurons.

Equation (17) governs the somatic membrane potential.
 The soma of a *Left* inhibitory interneuron only receives
 inhibitory input originating from the *Right* interneuron at
 the same spatial location:

$$C_m \frac{dS_i^L}{dt} - q_L^S (D_i^L - S_i^L) - f(S_i^L) = -(S_i^L + |E_{GABA}|) I_i^{RL}. \quad (17)$$

Local field potential (LFP) calculations

Local field potentials are calculated in the KinNeSS
 software package according to the methodology de-
 scribed in Versace et al. (2008). Emplacement of the
 electrode is determined by choosing a random location
 within [10–200]μm of the middle spatial location of
 the array of pyramidal layer 2/3 cells and aligning the
 electrode shank with the orientation of the cells. The
 distance of that electrode to the remaining 50 cells in
 the layer was uniformly random within the [10–1,000]μm
 interval. The electrode is composed of five equally spaced
 electrode tips covering the entire length of layer 2/3 cells
 (i.e., sum of the dendrite and soma lengths). The LFP
 output did not differ significantly across electrode tips,
 so the respective outputs were averaged together in
 order to get a global estimate. The Fast Fourier Transform
 (FFT) was calculated on the averaged LFP thereby
 obtained.

Synchronization measure

The synchronization measure described in Rosenberg et al.
 (1989) was used to quantify the significance of the coupling
 in a selected pair of layer 2/3 pyramidal cells in Fig. 9 (right
 column). Each spike train is divided into L segments of
 length T . Let τ_j represent spikes times, then the finite

1293 Fourier transform of the l^{th} segment at frequency ω is given
 1294 by:

$$d_N^T(\omega, l) = \sum_{(l-1)T \leq \tau_j \leq lT} e^{-i\omega\tau_j}. \quad (18)$$

1295 The cross-spectrum between two spike trains (denoted a
 1298 and b) is further given by:

$$\hat{f}_{ab}(\omega) = \frac{1}{2\pi LT} \sum_{l=1}^L d_a^T(\omega, l) \overline{d_b^T(\omega, l)}, \quad (19)$$

1300 where the bar indicates the complex conjugate. The squared
 1301 magnitude of the estimated coherency between the two
 1302 processes is defined as:

$$|R_{ab}(\omega)|^2 = \left| \frac{\hat{f}_{ab}(\omega)}{\hat{f}_{aa}(\omega)\hat{f}_{bb}(\omega)} \right|^2. \quad (20)$$

1303 An upper 95% confidence limit to test for the presence
 1306 of synchrony is given by $1 - (0.05)^{1/(L-1)}$. This limit is
 1307 plotted as a horizontal dashed line in Fig. 9. Values above
 1308 the line indicate significant coupling in the frequency range
 1309 indicated on the x-axis. Here $L=50$ and simulations were
 1310 run for 25,000 ms, such that $T=500$ ms, yielding a
 1311 frequency resolution of 2 Hz.

1312 Parameters

Q10 1313 *Network*

1314 Biophysical parameters for synaptic connections and cells
 1315 are given in Tables 3 and 4.

1316 *Weights and conduction delays*

1317 Horizontal weight kernels have a Gaussian shape as in
 1318 Eq. (13) (half-Gaussian for connections reaching interneur-
 1319 ons). The extent of the kernels is designed by dividing the
 1320 maximum extent of horizontal connections by the width of a
 1321 V1 hypercolumn (Yazdanbakhsh and Grossberg 2004).
 1322 Assuming a 7 mm wide kernel and a 1 mm wide
 1323 hypercolumn, the kernel size is set to 7 spatial locations.

1324 Horizontal axonal conduction delay kernels are linearly
 1325 dependent on distance, as in Eq. (14). The delay between
 1326 neighboring hypercolumns is calculated by dividing the
 1327 hypercolumn width by horizontal conduction speed. Recent
 1328 estimates of horizontal conduction speed in both monkey
 1329 V1 and cat area 17 put it at approximately 0.3 m/s
 1330 (Bringuier et al. 1999; Girard et al. 2001; Hirsch et al.
 1331 1991). Using a hypercolumn width of 1 mm, the conduc-

tion delay between neighboring hypercolumns is set to 1332
 3 ms; see Eq. (14). 1333

Simulation protocol 1334

All simulations were performed with KinNeSS (Versace et 1335
 al. 2008). Unless mentioned otherwise, firing rates are 1336
 measured once the network reaches a steady state, by 1337
 counting the number of spikes in the last second of 1338
 simulation. An integration time-step of 0.05 ms, 0.02 ms, 1339
 or 0.01 ms was used to obtain numerically accurate results. 1340
 All simulations took less than one hour on a dual 2 Ghz 1341
 AMD Opteron workstation with 4 Gb of RAM running 1342
 Linux. Unless mentioned otherwise, simulations were 1343
 conducted for 2,000 ms of simulated time. 1344

The results displayed in Figs. 6, 8 and 9 represent 1345
 averages (and standard deviation for error bars) from nine 1346
 different parameter settings where the maximal conduc- 1347
 tance of AMPA connections were varied along two 1348
 dimensions. Specifically, maximal conductance of the layer 1349
 4–2/3 connection was varied within the set {0.048, 0.049, 1350
 0.05} mS/cm² and maximal conductance of the layer 2/3- 1351
 interneuron connection was varied within the set {0.036, 1352
 0.037, 0.038} mS/cm². Results appeared qualitatively 1353
 similar in all cases. The simulations in Fig. 7 correspond 1354
 to the *middle* parameter configuration (i.e., values of 0.049 1355
 and 0.037 for respective parameters). 1356

In simulations where this is relevant, stimulus contrast is 1357
 defined as $X_i/0.0006$, where X_i is the current injected into 1358
 layer 4 pyramidal cells. Thus, nonlinearities between 1359
 stimulus contrast and current input to cortical cells are not 1360
 included in the simulations, implying that the simulations 1361
 of contrast-dependent data may arise totally due to 1362
 properties of the bipole network. 1363

Simulation of latency to first spike (Fig. 3(d)) 1364

The results displayed in Fig. 3(d) represents the difference 1365
 between illusory and real contours in the latency of the first 1366
 spike over the middle position of the contour, and for 1367
 various current input strengths. Nonzero input was applied 1368
 at locations 22 to 30 for real contours, whereas locations 25 1369
 to 27 were reset to zero for illusory contours. Current input 1370
 was set to 0.0084, 0.015, 0.021, 0.03, 0.045, 0.06, 0.075, 1371
 0.09, 0.105 and 0.12 nA. 1372

Simulation of bipole property (Fig. 5) 1373

Nonzero input was applied to units at spatial locations 1374
 21, 22, 23, 29, 30 and 31 in the ID input array. Input 1375
 strength at those locations was $X_i=0.03$ nA. The 1376
 simulation was conducted for 2,000 ms and firing rates 1377
 were calculated by monitoring spikes in the last 500 ms in 1378

1379 order to ensure that the network has settled into a stable
1380 firing mode.

1381 *Short-range completion simulations (Fig. 6)*

1382 Each stimulus bar is represented as an input (X_i) to a single
1383 location in Layer 4. This is motivated by considerations of
1384 recent estimates of the cortical magnification factor (cmf) at
1385 4° of eccentricity (Polimeni et al. 2006). Accordingly, a cmf
1386 of 2.7 mm° gives approximately 1 mm of cortical extent to
1387 a $30'$ stimulus bar as was used in the original study of
1388 Kapadia et al. (2000). However, 1–2 mm is the approximate
1389 diameter of one hypercolumn. Thus, a single stimulus bar is
1390 presented to a single location. This is also consistent with
1391 their adjustment of the length of the bars to the size of the
1392 CRFs. Stimulus contrasts of 20%, 30% and 50% were
1393 simulated by adjusting input strength to 0.012, 0.018 and
1394 0.03 nA, respectively.

1395 *Simulations of long-range modulation (Fig. 7)*

1396 The size of the bar stimuli in Polat et al. (1998) match CRF
1397 size which is here mapped to 3 adjacent columns. The
1398 distance between flanking bars is set to 7 locations, which is
1399 the shortest distance for which no inward completion
1400 occurred for the set of parameters considered. This particular
1401 constraint is in accordance with the method used in the
1402 original paper of Polat et al. (1998), and serves the purpose
1403 of studying long-range modulation instead of short-range
1404 completion. The current inputs simulated were (in nA):
1405 0.0036, 0.006, 0.0072, 0.0126, 0.021, 0.03, 0.06, 0.09 and
1406 0.12.

1407 *Outward propagation simulations (Fig. 8)*

1408 In the original study of Crook et al. (2002), each stimulus bar
1409 was simulated as input to a single location. In the original
1410 study, the separation between the target cell recorded and
1411 the cell whose CRF receives the flanking stimulus was
1412 ~ 2 mm. This corresponds to the approximate size of the cat's
1413 hypercolumn width (Lund et al. 2003). Thus, in the simu-
1414 lations the target and flanking bars were presented at adjacent
1415 locations. The target input strength was set to 0.0096 nA and
1416 that of the flanker line was set to 0.06 nA in order to approach
1417 the 1-to-10 contrast ratio in the original study.

1418 *Horizontal summation simulations (Fig. 9)*

1419 Arrays of collinear Gabor patches are represented by low
1420 contrast stimuli in the simulations. This is meant to
1421 represent the fact that the patches used in this study are of
1422 smaller diameter than the measured CRF size, such that
1423 they do not produce maximal activation. The length of stimuli

used is determined by using the cmf ($.21 \text{ mm}^\circ$) reported by 1424
the authors multiplied by the length (in degrees) of the original 1425
stimuli (here 5, 10, 15, 18, 23, 28 and 33 degrees). The 1426
corresponding array lengths are: 1, 2, 3, 4, 5, 6 and 7 mm, 1427
where each mm corresponds to one location in our simu- 1428
lations, which is in the order of the size of a hypercolumn in 1429
the tree shrew (Bosking 1997). For completeness, input 1430 Q12
stimuli are simulated at three contrast magnitudes by setting 1431
input strength to values of 0.0084, 0.0126 or 0.03 nA. The 1432
firing rate obtained is divided by the firing rate obtained for a 1433
13-units long bar of high contrast (input strength set to 1434
0.048 nA) simulated for the central parameter configuration 1435
in order to report quantities as relative activation with respect 1436
to a continuous bar of high contrast, consistent with the 1437
original study of Chisum et al. (2003). 1438

Fast resynchronization simulations (Fig. 10) 1439

The simulations of Fig. 10(a) and (b) were constructed by 1440
inserting a fixed random frame with input values ranging 1441
between 0 and 0.018 nA across spatial locations for the 1442
initial 100 ms and then switching to a homogeneous input 1443
stimulus for the remaining 900 ms. In the case of the full 1444
contour simulation (Fig. 10(a)), homogeneous input of 1445
magnitude 0.03 nA was applied to units 22 to 30. In the 1446
case of the illusory contour simulation (Fig. 10(b)), the same 1447
homogeneous input was applied to units 22, 23, 24, 28, 29 1448
and 30. Membrane potential traces of layer 2/3 bipole cells 1449
were low-pass filtered with a Butterworth filter of order 4 to 1450
remove single spikes but preserve slow oscillations, which 1451
simplifies detection of phase synchrony. Visual inspection of 1452
traces revealed that bursts occurred during ups and silent 1453
periods during troughs of the resulting filtered signals. The 1454
oscillations displayed therefore reliably represent burst 1455
occurrences. 1456

Oscillatory synchrony simulations (Fig. 11) 1457

Simulations were run for 25,000 ms. The full bar consisted of 1458
a 9-units wide stimulus. Separate bars consisted of 3-units 1459
wide stimuli, separated by a 3-units wide gap. The pair of cells 1460
selected for recording had their CRF located in the middle of 1461
each bar and were thus separated by 5 hypercolumns. This 1462
reflects the arrangement in the experimental recordings by 1463
Gray et al. (1989) where the pair of cortical cells was 1464
separated by approximately 7 mm. Input strength was set to 1465
0.03 nA. For the full bar and coherent bars condition, stimuli 1466
were presented with simultaneous injection in the layer 2/3 1467
dendrites of 10 ms sub-threshold white noise frames of 1468
amplitude varying in the interval $[0, 0.003]$ nA. For the 1469
incoherent bar condition, each short bar was presented for a 1470
randomly determined period of 300–500 ms. Each bar 1471
presentation was followed by a noise-only period of 300– 1472

1473 500 ms, whose purpose was to attenuate the periodicity
 1474 artificially induced in the delta band by the slow alternation
 1475 of stimulus bars. Note that, exclusion of these periods from
 1476 the simulation did not change the synchronization profile of
 1477 Fig. 11 (right) in the frequency bands of interest (mostly beta
 1478 and gamma). Furthermore, the cross-correlograms reported
 1479 in the middle column were shifted 100 ms in time to magnify
 1480 the signal strength for the incoherent bar condition. Indeed,
 1481 without this shift, the cross-correlogram output remains at 0
 1482 in the time frame considered for that condition, due to the
 1483 inclusion of noise-only frames. However, the pattern of result
 1484 remains the same when removing the shift. The coherence
 1485 index $|R|^2$ was calculated according to Eqs. (18)–(20).

1486 *LFP spectrum simulations (Fig. 12)*

1487 Simulations were run for 25,000 ms with 10 ms noise
 1488 frames. Static input was set to 0.012 nA and time-varying
 1489 noise magnitude spanned the interval [0 0.006] nA, such
 1490 that the signal-to-noise ratio varied from 0 to 50%. The
 1491 stimulus pattern simulated—i.e. a long bar, short bar,
 1492 flankers-only bar, etc.—did not significantly affect the
 1493 LFP power spectrum, whose peak varied in the upper
 1494 30 Hz to 50 Hz range. In the particular simulation shown in
 1495 Fig. 10, the stimulus pattern consisted of two 8 units wide
 1496 flankers separated by a 5 units wide gap, and noise
 1497 magnitude was set to 0 (no noise condition).

1498 *Threshold and analog sensitive single-cells (Fig. 13)*

1499 The plots A, B and C were generated from Eqs. (5)–(7)
 1500 using the phase plane technique described in Izhikevich
 1501 (2007), and for three representative current input levels (no
 1502 current, low current, large depolarizing current). Plot D was
 1503 generated by measuring the firing rate of a single neuron as
 1504 the current input to that neuron was increased from 0 nA.

1505 *Funding*

1506 All authors were partially supported by CELEST, a
 1507 National Science Foundation Science of Learning Center
 1508 [SBE-0354378]; S.G. and M.V. were partially supported by
 1509 the SyNAPSE program of the Defense Advanced Research
 1510 Project Agency [HR001109-03-0001]; and S.G. and J.L.
 1511 were also partially supported by the Defense Advanced
 1512 Research Project Agency [HR001-09-C-0011].

Q13 1513 **References**

1514 Amir, Y., Harel, M., & Malach, R. (1993). Cortical hierarchy reflected
 1515 in the organization of intrinsic connections in macaque monkey
 1516 visual cortex. *Journal of Comparative Neurology*, 334, 19–46.

Anzai, A., Peng, X., & Van Essen, D. C. (2007). Neurons in monkey
 1517 visual area V2 encode combinations of orientations. *Nature*
 1518 *Neuroscience*, 10, 1313–1321. 1519
 Bar, M., Kassam, K. S., Ghuman, A. S., Boshyan, J., Schmidt, A. M.,
 1520 Dale, A. M., et al. (2006). Top-down facilitation of visual
 1521 recognition. *Proceedings of the National Academy of Sciences*,
 1522 103, 449–454. 1523
 Berke, J. D., Hetrick, V., Breck, J., & Green, R. W. (2008). Transient
 1524 23- to 30-Hz oscillations in mouse hippocampus during
 1525 exploration of novel environments. *Hippocampus*, 18, 519–529. 1526
 Blasdel, G. G., & Lund, J. S. (1983). Termination of afferent axons in
 1527 macaque striate cortex. *Journal of Neuroscience*, 3, 1389–1413. 1528
 Bosking, W. H., Zhang, Y., Schofield, B., & Fitzpatrick, D. (1997).
 1529 Orientation selectivity and the arrangement of horizontal con-
 1530 nections in the tree shrew striate cortex. *Journal of Neuroscience*,
 1531 17, 2112–2127. 1532
 Boudreau, C. E., Williford, T. H., & Maunsell, H. R. (2006). Effects of
 1533 task difficulty and target likelihood in area V4 of macaque
 1534 monkeys. *Journal of Neurophysiology*, 96, 2377–2387. 1535
 Bringuier, V., Chavane, F., Glaeser, L., & Fregnac, Y. (1999).
 1536 Horizontal propagation of visual activity in the synaptic
 1537 integration field of area 17 neurons. *Science*, 283, 695–699. 1538
 Buffalo, E. A., Fries, P., & Desimone, R. (2004). *Layer-specific attentional*
 1539 *modulation in early visual areas. Program No. 717.6. 2004*
 1540 *Neuroscience Meeting Planner*. San Diego: Society for Neurosci-
 1541 ence. Online. Society for Neuroscience Abstracts, 30, 717–716. 1542
 Bullier, J., Hupé, J. M., James, A., & Girard, P. (1996). Functional
 1543 interactions between areas V1 and V2 in the monkey. *Journal of*
 1544 *Physiology - Paris*, 90, 217–220. 1545
 Buschman, T. J., & Miller, E. K. (2008). Covert shifts in attention by
 1546 frontal eye fields are synchronized to population oscillations.
 1547 Submitted for publication. 1548
 Callaway, E. M., & Wiser, A. K. (1996). Contributions of individual
 1549 layer 2–5 spiny neurons to local circuits in macaque primary
 1550 visual cortex. *Visual Neuroscience*, 13, 907–922. 1551
 Cao, Y., & Grossberg, S. (2005). A laminar cortical model of
 1552 stereopsis and 3D surface perception: closure and da Vinci
 1553 stereopsis. *Spatial Vision*, 18, 515–578. 1554
 Carpenter, G. A. (1979). Bursting phenomena in excitable membranes.
 1555 *SIAM Journal of Applied Mathematics*, 36, 334–372. 1556
 Carpenter, G., & Grossberg, S. (1993). Normal and amnesic learning,
 1557 recognition, and memory by a neural model of cortico-
 1558 hippocampal interactions. *Trends in Neurosciences*, 16, 131–137. 1559
 Chisum, H. J., Mooser, F., & Fitzpatrick, D. (2003). Emergent
 1560 properties of layer 2/3 neurons reflect the collinear arrangement
 1561 of horizontal connections in tree shrew visual cortex. *Journal of*
 1562 *Neuroscience*, 23, 2947–2960. 1563
 Cohen, M. A., & Grossberg, S. (1984). Neural dynamics of brightness
 1564 perception: features, boundaries, diffusion, and resonance. *Per-
 1565 ception & Psychophysics*, 36, 428–456. 1566
 Crook, J. M., Engelmann, R., & Löwel, S. (2002). GABA-inactivation
 1567 attenuates collinear facilitation in cat primary visual cortex.
 1568 *Experimental Brain Research*, 143, 295–302. 1569
 Domijan, D., Šetic, M., & Švegar, D. (2007). A model of illusory
 1570 contour formation based on dendritic computation. *Neurocom-
 1571 puting*, 70, 1977–1982. 1572
 Eckhorn, R., Bauer, R., Jordan, W., Brosch, M., Kruse, W., Munk, M., et
 1573 al. (1988). Coherent oscillations: a mechanism of feature linking in
 1574 the visual cortex? *Biological Cybernetics*, 60, 121–130. 1575
 Elston, G. N., Rosa, G. P., & Calford, M. B. (1996). Comparison of
 1576 dendritic fields of Layer III pyramidal neurons in striate and
 1577 extrastriate visual areas of the marmoset: a lucifer yellow
 1578 intracellular injection study. *Cerebral Cortex*, 6, 807–813. 1579
 Ernst, U., Pawelzik, K., & Geisel, T. (1995). Synchronization induced
 1580 by temporal delays in pulse-couple oscillators. *Physical Review*
 1581 *Letters*, 74, 1570–1573. 1582

- 1583 Fang, L., & Grossberg, S. (2009). From stereogram to surface: how
1584 the brain sees the world in depth. *Spatial Vision*, 22, 45–82.
- 1585 Ferster, D., Chung, S., & Wheat, H. (1996). Orientation selectivity of
1586 thalamic input to simple cells of cat visual cortex. *Nature*, 380,
1587 249–252.
- 1588 Field, D. J., Hayes, A., & Hess, R. F. (1993). Contour integration by
1589 the human visual system—evidence for a local association field.
1590 *Vision Research*, 33, 173–193.
- 1591 Fitzhugh, R. (1955). Mathematical models of threshold phenomena in the
1592 nerve membrane. *Bulletin of Mathematical Biology*, 17, 252–278.
- 1593 Fitzpatrick, D. (1996). The functional organization of local circuits in
1594 visual cortex: insights from the study of tree shrew striate cortex.
1595 *Cerebral Cortex*, 6, 329–341.
- 1596 Francis, G., Grossberg, S., & Mingolla, E. (1994). Cortical dynamics
1597 of feature binding and reset: control of visual persistence. *Vision
1598 Research*, 34, 1089–1104.
- 1599 Fries, P., Reynolds, J. H., Rorie, A. E., & Desimone, R. (2001).
1600 Modulation of oscillatory neuronal synchronization by selective
1601 visual attention. *Science*, 291, 1560–1563.
- 1602 Fukuda, T., Kosaka, T., Singer, W., & Galuske, R. A. W. (2006). Gap
1603 junctions among dendrites of cortical GABAergic neurons
1604 establish a dense and widespread intercolumnar network. *Journal
1605 of Neuroscience*, 26, 3434–3443.
- 1606 Gautrais, J., & Thorpe, S. (1998). Rate coding versus temporal order
1607 coding: a theoretical approach. *Biosystems*, 48, 57–65.
- 1608 Gerstner, W. (1996). Rapid phase locking in systems of pulse-coupled
1609 oscillators with delays. *Physical Review Letters*, 76, 1755–1758.
- 1610 Gilbert, C. D., & Wiesel, T. N. (1983). Clustered intrinsic connections
1611 in cat visual cortex. *Journal of Neuroscience*, 3, 1116–1133.
- 1612 Girard, P., Hupé, J. M., & Bullier, J. (2001). Feedforward and
1613 feedback connections between areas V1 and V2 of the monkey have
1614 similar rapid conduction velocities. *Journal of Neurophysiology*, 85,
1615 1328–1331.
- 1616 Golubitsky, M., & Stewart, I. (2006). Nonlinear dynamics of
1617 networks: the groupoid formalism. *Bulletin of the American
1618 Mathematical Society*, 43, 305–364.
- 1619 Gray, C. M., & Singer, W. (1989). Stimulus-specific neuronal
1620 oscillations in orientation columns of cat visual cortex. *Proceedings
1621 of the National Academy of Sciences USA*, 86, 1698–1702.
- 1622 Gray, C. M., König, P., Engel, A. K., & Singer, W. (1989). Oscillatory
1623 responses in cat visual cortex exhibit inter-columnar synchroniza-
1624 tion which reflects global stimulus properties. *Nature*, 338, 334–
1625 337.
- 1626 Gregoriou, G. G., Gotts, S. J., Zhou, H., & Desimone, R. (2009).
1627 High-frequency, long-range coupling between prefrontal and
1628 visual cortex during attention. *Science*, 324, 1207–1210.
- 1629 Grossberg, S. (1973). Contour enhancement, short term memory, and
1630 constancies in reverberating neural networks. *Studies in Applied
1631 Mathematics*, 52, 217–257. Reprinted in *Studies of Mind and
1632 Brain*, S. Grossberg (1982). D. Reidel Publishing Company:
1633 Dordrecht, Holland.
- 1634 Grossberg, S. (1976a). Adaptive pattern classification and universal
1635 recoding, I: parallel development and coding of neural feature
1636 detectors. *Biological Cybernetics*, 23, 121–134.
- 1637 Grossberg, S. (1976b). Adaptive pattern classification and universal
1638 recoding, II: feedback, expectation, olfaction, and illusions.
1639 *Biological Cybernetics*, 23, 187–202.
- 1640 Grossberg, S. (1980). How does a brain build a cognitive code?
1641 *Psychological Review*, 87, 1–51.
- 1642 Grossberg, S. (1984). Outline of a theory of brightness, color, and
1643 form perception. In E. Degreef & J. van Buggenhout (Eds.),
1644 *Trends in mathematical psychology* (pp. 59–85). Amsterdam:
1645 North-Holland.
- 1646 Grossberg, S. (1999). How does the cerebral cortex work? Learning,
1647 attention, and grouping by the laminar circuits of visual cortex.
1648 *Spatial Vision*, 12, 163–185.
- Grossberg, S. (2003). How does the cerebral cortex work? Develop- 1649
ment, learning, attention, and 3D vision by laminar circuits of 1650
visual cortex. *Behavioral and Cognitive Neuroscience Reviews*, 1651
2, 47–76.
- Grossberg, S. (2007). Consciousness CLEARs the mind. *Neural 1653
Networks*, 20, 1040–1053.
- Grossberg, S. (2009). Beta oscillations and hippocampal place cell 1655
learning during exploration of novel environments. *Hippocampus*, 1656
in press.
- Grossberg, S., & Grunewald, A. (1997). Cortical synchronization and 1658
perceptual framing. *Journal of Cognitive Neuroscience*, 9, 117–
1659 132.
- Grossberg, S., & Mingolla, E. (1985a). Neural dynamics of perceptual 1661
grouping: textures, boundaries, and emergent segmentations. 1662
Perception & Psychophysics, 38, 141–171.
- Grossberg, S., & Mingolla, E. (1985b). Neural dynamics of form 1664
perception: boundary completion, illusory figures, and neon color 1665
spreading. *Psychological Review*, 92, 173–211.
- Grossberg, S., & Raizada, R. D. S. (2000). Contrast-sensitive 1667
perceptual grouping and object-based attention in the laminar 1668
circuits of primary visual cortex. *Vision Research*, 40, 1413–
1669 1432.
- Grossberg, S., & Somers, D. (1991). Synchronized oscillations during 1671
cooperative feature linking in a cortical model of visual 1672
perception. *Neural Networks*, 4, 453–466.
- Grossberg, S., & Swaminathan, G. (2004). A laminar cortical model 1674
of 3D perception of slanted and curved surfaces and of 2D 1675
images: development, attention and bistability. *Vision Research*, 1676
44, 1147–1187.
- Grossberg, S., & Todorović, D. (1988). Neural dynamics of 1-D and 1678
2-D brightness perception: a unified model of classical and recent 1679
phenomena. *Perception & Psychophysics*, 43, 241–277.
- Grossberg, S., & Versace, M. (2008). Spikes, synchrony, and attentive 1680
learning by laminar thalamocortical circuits. *Brain Research*, 1681
1218, 278–312.
- Grossberg, S., & Williamson, J. R. (2001). A neural model of how 1684
horizontal and interlaminar connections of visual cortex develop 1685
into adult circuits that carry out perceptual grouping and learning. 1686
Cerebral Cortex, 11, 37–58.
- Grossberg, S., & Yazdanbakhsh, A. (2005). Laminar cortical dynamics 1688
of 3D surface perception: stratification, transparency, and neon 1689
color spreading. *Vision Research*, 45, 1725–1743.
- Grossberg, S., Mingolla, E., & Ross, W. D. (1997). Visual brain and 1691
visual perception: how does the cortex do perceptual grouping? 1692
Trends in Neuroscience, 20, 106–111.
- Grossberg, S., Yazdanbakhsh, A., Cao, Y., & Swaminathan, G. (2008). 1694
How does binocular rivalry emerge from cortical mechanisms of 1695
3-D vision? *Vision Research*, 48, 2232–2250.
- Guttman, S., Sekuler, A., & Kellman, P. J. (2003). Temporal variations 1697
in visual completion: a reflection of spatial limits? *Journal of
1698 Experimental Psychology: Human Perception and Performance*, 1699
29, 1211–1227.
- Halgren, E., Mendola, J., Chong, C. D. R., & Dale, A. M. (2003). 1701
Cortical activation to illusory shapes as measured with magneto- 1702
encephalography. *Neuroimage*, 18, 1001–1009.
- Heeger, D. J. (1992). Normalization of cell responses in cat striate 1703
cortex. *Visual Neuroscience*, 9, 181–197.
- Hirsch, J. A., & Gilbert, C. D. (1991). Synaptic physiology of 1706
horizontal connections in the cat's visual cortex. *Journal of
1707 Neuroscience*, 11, 1800–1809.
- Hochstein, S., & Ahissar, M. (2002). View from the top: hierarchies 1709
and reverse hierarchies in the visual system. *Neuron*, 36, 791–
1710 804.
- Hodgkin, A. L., & Huxley, A. F. (1952). A quantitative description of 1712
membrane current and its application to conduction and 1713
excitation in nerve. *Journal of Physiology*, 117, 500–544. 1714

- 1715 Holmgren, C., Harkany, T., Svennenfors, B., & Zilberter, Y. (2003).
1716 Pyramidal cell communication within local networks in layer 2/3
1717 of rat neocortex. *Journal of Physiology*, *551*, 139–153.
- 1718 Hupé, J.-M., James, A. C., Girard, P., Lomber, S. G., Payne, B. R., &
1719 Bullier, J. (2001). Feedback connections act on the early part of
1720 the responses in monkey visual cortex. *Journal of Neurophysiology*,
1721 *85*, 134–145.
- 1722 Izhikevich, E. (2007). *Dynamical systems in neuroscience*. Cambridge:
1723 MIT.
- 1724 Kapadia, M., Westheimer, G., & Gilbert, C. D. (2000). Spatial
1725 distribution of contextual interactions in primary visual cortex and
1726 in visual perception. *Journal of Neurophysiology*, *84*, 2048–2062.
- 1727 Kellman, P. J., & Shipley, T. F. (1991). A theory of visual interpolation in
1728 object perception. *Cognitive Psychology*, *23*, 141–221.
- 1729 Kisvárdy, Z. F., Tóth, É., Rausch, M., & Eysel, U. T. (1997).
1730 Orientation-specific relationship between populations of excitatory
1731 and inhibitory lateral connections in the visual cortex of the cat.
1732 *Cerebral Cortex*, *7*, 605–618.
- 1733 Koch, C. (1999). *Biophysics of computation: information processing*
1734 *in single neurons*. New York: Oxford University Press.
- 1735 Köhn, J., & Wörgöter, F. (1998). Employing the Z-transform to
1736 optimize the calculation of the synaptic conductance of NMDA
1737 and other synaptic channels in network simulations. *Neural*
1738 *Computation*, *10*, 1639–1651.
- 1739 Lamme, V. A. F., & Roelfsema, P. R. (2000). The distinct modes of
1740 vision offered by feedforward and recurrent processing. *Trends in*
1741 *Neuroscience*, *23*, 571–579.
- 1742 Lamme, V. A. F., Rodriguez-Rodriguez, V., & Spekreijse, H. (1999).
1743 Separate processing dynamics for texture elements, boundaries
1744 and surfaces in primary visual cortex of the macaque monkey.
1745 *Cerebral Cortex*, *9*, 406–413.
- 1746 Leshner, G. W., & Mingolla, E. (1993). The role of edges and line-ends
1747 in illusory contour formation. *Vision Research*, *33*, 2253–2270.
- 1748 Levitt, J. B., Yoshioka, T., & Lund, J. S. (1994). Intrinsic cortical
1749 connections in macaque visual area V2: evidence for interaction
1750 between different functional streams. *Journal of Comparative*
1751 *Neurology*, *342*, 551–570.
- 1752 Li, Z. (1998). A neural model of contour integration in the primary
1753 visual cortex. *Neural Computation*, *10*, 903–940.
- 1754 Lund, J. S., Griffiths, S., Rumberger, A., & Levitt, J. B. (2001).
1755 Inhibitory synapse cover on the somata of excitatory neurons in
1756 macaque monkey visual cortex. *Cerebral Cortex*, *11*, 783–795.
- 1757 Lund, J. S., Angelucci, A., & Bressloff, P. C. (2003). Anatomical
1758 substrates for functional columns in macaque monkey primary
1759 visual cortex. *Cerebral Cortex*, *12*, 15–24.
- 1760 McGuire, B. A., Gilbert, C. D., Rivlin, P. K., & Wiesel, T. N. (1991).
1761 Targets of horizontal connections in macaque primary visual
1762 cortex. *Journal of Comparative Neurology*, *305*, 370–392.
- 1763 Megias, M., Emri, Z., Freund, T. F., & Gulyás, A. I. (2001). Total
1764 number and distribution of inhibitory and excitatory synapses on
1765 hippocampal CA1 pyramidal cells. *Neuroscience*, *102*, 527–540.
- 1766 Meyer, G., & Ming, C. (1988). The visible persistence of illusory
1767 contours. *Canadian Journal of Psychology*, *42*, 479–488.
- 1768 Milner, P. A. (1974). A model for visual shape recognition.
1769 *Psychological Review*, *81*, 5221–5525.
- 1770 Murray, R. F., Sekuler, A. B., & Bennett, P. J. (2001). Time course of
1771 amodal completion revealed by a shape discrimination task.
1772 *Psychonomics Bulletin & Review*, *8*, 713–720.
- 1773 Murray, M. M., Wylie, G. R., Higgins, B. A., Javitt, D. C., Schroeder,
1774 C. E., & Foxe, J. J. (2002). The spatiotemporal dynamics of
1775 illusory contour processing: combined high-density electrical
1776 mapping, source analysis, and functional magnetic resonance
1777 imaging. *Journal of Neuroscience*, *22*, 5055–5073.
- 1778 Oram, M. W., & Perrett, D. I. (1992). Time course of neural responses
1779 discriminating different views of the face and head. *Journal of*
1780 *Neurophysiology*, *68*, 70–84.
- Peterhans, E., & Von Der Heydt, R. (1989). Mechanisms of contour
1781 perception in monkey visual cortex II. Contour bridging gaps.
1782 *Journal of Neuroscience*, *9*, 1749–1763.
- 1783 Polat, U., Mizobe, K., Pettet, M. W., Kasamatsu, T., & Norcia, A. M.
1784 (1998). Collinear stimuli regulate visual responses depending on
1785 cell's contrast threshold. *Nature*, *391*, 580–584.
- 1786 Polimeni, J., Balasubramanian, M., & Schwartz, E. L. (2006). Multi-
1787 area visuotopic map complexes in macaque striate and extra-
1788 striate cortex. *Vision Research*, *46*, 3336–3359.
- 1789 Polsky, A., Mel, B. W., & Schiller, J. (2004). Computational subunits
1790 in thin dendrites of pyramidal cells. *Nature Neuroscience*, *7*,
1791 621–627.
- 1792 Raizada, R. D. S., & Grossberg, S. (2001). Context-sensitive bindings
1793 by the laminar circuits of V1 and V2: a unified model of
1794 perceptual grouping, attention and orientation contrast. *Visual*
1795 *Cognition*, *8*, 431–466.
- 1796 Ringach, D. L., & Shapley, R. (1996). Spatial and temporal properties
1797 of illusory contours and amodal boundary completion. *Vision*
1798 *Research*, *36*, 3037–3050.
- 1799 Rosenberg, J. R., Amjad, A. M., Breeze, P., Brillinger, D. R., &
1800 Halliday, D. M. (1989). The Fourier approach to the identification of
1801 functional coupling between neuronal spike trains. *Progress in*
1802 *Biophysics and Molecular Biology*, *53*, 1–31.
- 1803 Salin, P., & Bullier, J. (1995). Corticocortical connections in the visual
1804 system: structure and function. *Physiological Reviews*, *75*, 107–
1805 154.
- 1806 Samonds, J. M., Zhou, Z., Bernard, M. R., & Bonds, A. B. (2006).
1807 Synchronous activity in visual cortex encodes collinear and
1808 cocircular contours. *Journal of Neurophysiology*, *95*, 2602–2616.
- 1809 Sandell, J. H., & Schiller, P. H. (1982). Effect of cooling area 18 on
1810 striate cortex cells in the squirrel monkey. *Journal of Neuro-*
1811 *physiology*, *48*, 38–48.
- 1812 Sarpeshkar, R. (1998). Analog versus digital: extrapolating from
1813 electronics to neurobiology. *Neural Computation*, *10*, 1601–
1814 1638.
- 1815 Schmidt, K. E., Goebel, R., Löwel, S., & Singer, W. (1997). The
1816 perceptual grouping criterion of colinearity is reflected by
1817 anisotropies of connections in the primary visual cortex.
1818 *European Journal of Neuroscience*, *9*, 1083–1089.
- 1819 Segev, I. (1998). Cable and compartmental models of dendritic trees.
1820 In J. M. Bower & D. Beeman (Eds.), *The book of genesis*. New
1821 York: Springer-Verlag/TELOS.
- 1822 Sekuler, A. B., & Palmer, S. E. (1992). Perception of partly occluded
1823 objects: a microgenetic analysis. *Journal of Experimental*
1824 *Psychology: General*, *121*, 95–111.
- 1825 Shmuel, A., Korman, M., Sterkin, A., Harel, M., Ullman, S., Malach,
1826 R., et al. (2005). Retinotopic axis specificity and selective
1827 clustering of feedback projections from V2 to V1 in the Owl
1828 monkey. *Journal of Neuroscience*, *23*, 2117–2131.
- 1829 Silito, A. N., Jones, H. E., Gerstein, G. L., & West, D. C. (1994).
1830 Feature-linked synchronization of thalamic relay cell firing
1831 induced by feedback from the visual cortex. *Nature*, *369*, 479–
1832 482.
- 1833 Soriano, M., Spillmann, L., & Bach, M. (1996). The abutting grating
1834 illusion. *Vision Research*, *36*, 109–116.
- 1835 Spruston, N. (2008). Pyramidal neurons: dendritic structure and
1836 synaptic integration. *Nature Reviews Neuroscience*, *9*, 206–221.
- 1837 Stetter, D. D., Das, A., Bennett, J., & Gilbert, C. D. (2002). Lateral
1838 connectivity and contextual interactions in macaque primary
1839 visual cortex. *Neuron*, *36*, 739–750.
- 1840 Tallon, C., Bertrand, O., Bouchet, P., & Pernier, J. (1995). Gamma-range
1841 activity evoked by coherent visual stimuli in humans. *European*
1842 *Journal of Neuroscience*, *7*, 1285–1291.
- 1843 Tamas, G., Somogyi, P., & Buhl, E. H. (1998). Differentially
1844 interconnected networks of GABAergic interneurons in the visual
1845 cortex of the cat. *Journal of Neuroscience*, *18*, 4255–4270.
- 1846

- 1847 Thomson, A. M., & Bannister, A. P. (2003). Interlaminar connections 1864
1848 in the neocortex. *Cerebral Cortex*, *13*, 5–14. 1865
- 1849 Thorpe, S., Delorme, A., & Van Rullen, R. (2001). Spike-based 1866
1850 strategies for rapid processing. *Neural Networks*, *14*, 715–725. 1867
- 1851 Traub, R. D., & Miles, R. (1991). *Neuronal networks of the* 1868
1852 *hippocampus*. Cambridge: Cambridge University Press. 1869
- 1853 Tusa, R. J., Rosenquist, A. C., & Palmer, L. A. (1979). Retinotopic 1870
1854 organization of areas 18 and 19 in the cat. *Journal of* 1871
1855 *Comparative Neurology*, *185*, 657–678. 1872
- 1856 VanRullen, R., Delorme, A., & Thorpe, S. J. (2001). Feed-forward 1873
1857 contour integration in primary visual cortex based on asynchronous 1874
1858 spike propagation. *Neurocomputing*, *38–40*, 1–4. 1875
- 1859 VanRullen, R., Guyonneau, P., & Thorpe, S. J. (2005). Spike times 1876
1860 make sense. *Trends in Neuroscience*, *28*, 1–4. 1877
- 1861 Versace, M., Ames, H., Léveillé, J., Fortenberry, B., Mhatre, H., & 1878
1862 Gorchetchnikov, A. (2008). KInNeSS: a modular framework for 1879
1863 computational neuroscience. *Neuroinformatics*, *6*, 291–309. 1880
- 1881 von der Heydt, R., Peterhans, E., & Baumgartner, G. (1984). Illusory 1864
1865 contours and cortical neuron responses. *Science*, *224*, 1260–1262. 1866
- 1867 von der Malsburg, C. (1981). *The correlation theory of brain function*. 1868
1869 Göttingen: Internal Report 81-2, Dept. of Neurobiology, Max- 1870
1871 Planck Institute for Biophysical Chemistry. 1872
- 1873 Yazdanbakhsh, A., & Grossberg, S. (2004). Fast synchronization of 1874
1875 perceptual grouping in laminar visual cortical circuits. *Neural* 1876
1877 *Networks*, *17*, 707–718. 1878
- 1879 Yen, S.-C., & Finkel, L. H. (1998). Extraction of perceptually salient 1880
1881 contours by striate cortical networks. *Vision Research*, *38*, 719–741. 1882
- 1883 Yen, S.-C., Menschik, E. D., & Finkel, L. H. (1999). Perceptual 1884
1885 grouping in striate cortical networks mediated by synchronization 1886
1887 and desynchronization. *Neurocomputing*, *26–27*, 609–616. 1888
- 1889 Yoshino, A., Kawamoto, M., Yoshida, T., Kobayashi, N., Shigemura, 1890
1891 J., Takahashi, Y., et al. (2006). Activation time course of 1892
1893 responses to illusory contours and salient region: a high-density 1894
1895 electrical mapping comparison. *Brain Research*, *1071*, 137–144. 1896

UNCORRECTED PROOF